

Bistability of the climate around the habitable zone: a thermodynamic investigation

Robert Boschi^a, Valerio Lucarini^{a,b}, Salvatore Pascale^a

^a*Klimacampus, Meteorologisches Institut, Universität Hamburg, Hamburg, Germany*

^b*Department of Mathematics and Statistics, University of Reading, Reading, UK*

Abstract

The goal of this paper is to explore the potential multistability of the climate of a planet around the habitable zone. We apply our methodology to the Earth system, but our investigation has more general relevance. A thorough investigation of the thermodynamics of the climate system is performed for very diverse conditions of energy input and infrared atmosphere opacity. Using PlaSim, an Earth-like general circulation model, the solar constant S^* is modulated between 1160 and 1510 Wm^{-2} and the CO_2 concentration, $[\text{CO}_2]$, from 90 to 2880 ppm. It is observed that in such a parameter range the climate is bistable, i.e. there are two coexisting attractors, one characterised by warm, moist climates (W) and one by completely frozen sea surface (Snowball Earth, SB). Linear relationships are found for the two transition lines ($W \rightarrow \text{SB}$ and $\text{SB} \rightarrow W$) in $(S^*, [\text{CO}_2])$ between S^* and the logarithm of $[\text{CO}_2]$. The dynamical and thermodynamical properties – energy fluxes, Lorenz energy cycle, Carnot efficiency, material entropy production – of the W and SB states are very different: W states are dominated by the hydrological cycle and latent heat is prominent in the material entropy production; the SB states are eminently dry climates where heat transport is realized through sensible heat fluxes and entropy mostly generated by dissipation of kinetic energy. We also show that the Carnot efficiency regularly increases towards each transition between W and SB, with a large decrease in each transition. Finally, we propose well-defined empirical functions allowing for expressing the global non-equilibrium thermodynamical properties of the system in terms of either the mean surface temperature or the mean planetary emission temperature. This paves the way for the possibility of proposing efficient parametrisations of complex non-equilibrium properties and of practically deducing fundamental properties of a planetary system

from a relatively simple observable.

Keywords: bistability, non-equilibrium thermodynamics, climatic shift, snowball earth, habitable zone

2010 MSC: 85A20, 80A17, 86A10, 76U05, 37G35

1. Introduction

1.1. Planetary atmospheres and extrasolar planets

A very active recent field of research in astrophysical sciences is the observational, model-assisted, and theoretical investigation of extra-solar planetary objects. In less than two decades, the development of new instruments have lead to the detection of the first extra-solar planet in the mid 90s to more and more refined observations of the characteristics of several hundreds of such bodies. The properties of planets vary greatly, in terms of their compositions - gaseous or rocky -, nature of their atmosphere, and of their size - ranging in several orders of magnitude. Astronomical and astrophysical factors of great relevance include the temperature and the intensity of the radiation emitted by the parent star, the orbital parameters, and whether or not the planet is tidally locked. A great deal of effort has been directed at constraining the combinations of physical configurations potentially compatible with life (habitable zone) , that is to say with the possibility of observing water prominently or at least partially in its liquid form at surface. Obviously, the so-called habitable zone is the setting where we can hope to find forms of extraterrestrial life, at least assuming that life necessarily expresses itself in forms analogous to those we experience on our planet. Recently, ESOs HARPS planet finder estimated that just in the Milky Way billions of habitable Earth-like rocky planets could orbit around faint red dwarfs, with in the order of one hundred in the immediate vicinity of our Solar system (Bonfils and coauthors, 2012). We refer the reader to the website (<http://exoplanet.eu/index.php>) – which is dedicated to collecting information on all newly discovered planets and on the related bibliography – and recently published books (Dvorak, 2008; Saeger, 2010; Kasting, 2009; Perryman, 2011).

A great deal of interest is now being paid to inferring, studying, and the modeling of planetary atmospheres, i.e., in the case of rocky planets, the fluid envelope that surrounds the planet and the response to the differential

31 heating due to the absorption of the incoming radiation. Planetary atmo-
 32 spheres may feature complex chemical compositions and be characterised by
 33 the relevant presence of phase transitions of some of the components, which
 34 may have large effects on the radiative properties. The geometry describ-
 35 ing how the planet and its parent star face each other determines to a first
 36 approximation the horizontal inhomogeneities, whereas the atmospheric op-
 37 tical properties, and in particular its opacity to the incoming radiation, has
 38 an effect on the vertical structure (e.g. Earth's the optically thin atmosphere
 39 is typically heated from the planets surface). The general circulation of the
 40 planetary atmosphere is powered, just like a Carnot engine by such inhom-
 41 geneities with, on average, heating occurring at higher temperatures being
 42 then removed in cooler regions. The circulation acts to reduce the temper-
 43 ature gradients through transport processes, and on average the generation
 44 of kinetic energy is compensated by its irreversible dissipation through vis-
 45 cous processes. Irreversible heat transport and dissipation, and processes of
 46 radiation absorption and emission contribute to the generation of entropy.
 47 The steady state is realised by balancing energy and entropy fluxes between
 48 the planetary atmosphere and the surrounding space. Various aspects of this
 49 closed chain of interdependent processes have been described for terrestrial
 50 conditions (Lorenz, 1967; Peixoto and Oort, 1992; Held and Soden, 2006;
 51 Lucarini, 2009; Lucarini et al., 2011), but these arguments could be applied
 52 to planetary atmospheres more generally.

53 The recent discoveries in planetary astronomy and astrophysics are pro-
 54 gressively affecting classical geophysical sciences (by definition Earth-centered).
 55 The study of, e.g. Jupiters or Venus general circulation has a rather old his-
 56 tory, but with the recent and foreseeable future discoveries of exoplanets we
 57 have the opportunity of facing a vast variety of planetary configurations, so
 58 that we are going from considering special cases of climates (Earth, Jupiter,
 59 Saturn, etc), to being able to study a quasi-continuous distribution of cli-
 60 mates in some parametric space. Following Read (2011), one should note
 61 that it is possible to reduce the variety of climate settings by adopting the
 62 fluid-dynamical classical method of similarity, i.e. by defining a set of di-
 63 mensionless numbers that fully characterise the climate states. When two
 64 climate states share the same set of dimensionless numbers, they are dynam-
 65 ically equivalent, so that the statistical properties of one can be mapped into
 66 those of the other one with simple algebraic operations. At this stage, we
 67 are left with two additional elements to cope with:

- 68 • how to characterise succinctly a climatic state, conveying minimal but
69 comprehensive physical information: the planetary atmospheres are,
70 in general, turbulent fluids with variability on a very vast of range of
71 spatial and temporal scales?
- 72 • how to verify, at least approximately, the validity of our simulations
73 and of our theoretical understanding of the planetary circulations we
74 are able to model?

75 The two items are closely related to the definition of robust observables.
76 Energy conservation imposes that the incoming radiation onto a planet is
77 instantaneously equal to the sum of the radiation that is absorbed and scat-
78 tered by the planet. Assuming steady state, when averaging over a suffi-
79 ciently long time interval, the radiation absorbed by the planet is equal to
80 the radiation the planet emits off to space. These quantities allow defining
81 the average albedo of the planet and its effective thermodynamic temper-
82 ature, which constitute the most fundamental description of the properties
83 of the planet in terms of the first law of thermodynamics. The observation
84 of a planet as represented by a single pixel recorded by a telescope permits
85 to gather information at this level of detail in terms of its overall macro-
86 scopic properties. Obviously, the observations provide much more than this,
87 such as the spectrum emitted by the planet (and by the star). Nonetheless,
88 in terms of the macroscopic thermodynamic properties of the planet, only
89 the spectrally integrated quantities are mostly relevant. Under conditions
90 of steady state, given the inhomogeneity of the incoming radiation and of
91 the boundary conditions, the vanishing net energy budget at the top of the
92 atmosphere (TOA) results from the cancellation between regions where the
93 budget is positive and regions where the budget is negative (low and mid-
94 high latitudes regions, in the case of the Earth). Steady state argument
95 imply that the absolute value of the imbalance in either region is equal to
96 the energy transmitted from the regions where the energy balance at the top
97 of the atmosphere is positive from those where such balance is negative, and
98 the transport is performed across the atmospheric fluid envelope through
99 material transport and horizontal deflection of the incoming radiation (in
100 the case of very thick atmospheres). Note that the correct representation of
101 these large scale properties in state-of-the-art models of the Earth's climate
102 is far from being a trivial task (Lucarini and Ragone, 2011).

103 Moreover, the second law of thermodynamics imposes that the regions
104 featuring positive TOA energy budget are warmer (i.e. their total emitted

105 radiation is larger) than those where the balance is negative. One can show
 106 that the entropy production due to such irreversible transport of energy from
 107 hot to cold regions gives a lower bound to the total material entropy pro-
 108 duction of the planet. Moreover, it is possible to provide a lower bound to
 109 the total dissipation of kinetic energy or, equivalently, to the intensity of the
 110 Lorenz energy cycle (Lucarini et al., 2011). This discussion implies that if a
 111 telescope allows for an observational resolution involving more than one pixel,
 112 able to distinguish between warmer and colder regions, it is possible to de-
 113 rive fundamental information on the macroscopic thermodynamic properties
 114 of the planet in terms of the 2nd law of thermodynamics. This brief discus-
 115 sion suggests that non-equilibrium thermodynamics provides rather powerful
 116 methods and concepts for analysing the fundamental properties of plane-
 117 tary atmospheres, for testing models performances, and for deriving bounds
 118 on the physical properties of the system even when low-resolution data are
 119 available. Following previous work in the field (Pujol, 2003; Fraedrich and
 120 Lunkeit, 2008; Lucarini, 2009; Lucarini et al., 2010b, 2011; Pascale et al.,
 121 2011a,b; Li and Chylek, 2012), we propose to use this framework in order
 122 to study planetary atmospheres in a rather general setting of forcings and
 123 boundary conditions.

124 1.2. *Habitability conditions and climatic bistability*

125 As mentioned above, a great deal of interest in the investigation of plan-
 126 etary atmospheres is directed at studying conditions within or about the
 127 Habitable zone. Nonetheless, being in the the Habitable zone is a *necessary*
 128 *but not a sufficient condition* for a planet to have liquid water at the surface,
 129 even if the chemical composition of the atmosphere would in principle allow
 130 for it. In fact, the paleohistory of our planet provides strong evidence of the
 131 fact that the astronomical and astrophysical parameters of the Sun-Earth sys-
 132 tem support two distinct steady states, the warm state (W) characterised by
 133 widespread liquid water, and one, instead, characterised by the global glacia-
 134 tion of water and an extremely dry atmosphere, i.e. the so-called Snowball
 135 state (SB). What we propose here is a thorough investigation of these two
 136 states in a bidimensional parameteric space, with the goal of detailing the
 137 region of bistability of the Earth system and analysing the bifurcation points
 138 and the mechanisms of transitions between the two states. Our investigation
 139 deals with Earth conditions because this is the only system where an exten-
 140 sive body of literature – observational, theoretical, and model-assisted – on

141 the Snowball state and the Snowball-Snowfree transitions is available, but
142 our scope is much wider.

143 Probably the most notable examples of climate change events occurred
144 during the Neoproterozoic (period spanning from 1000 million to 540 million
145 years ago), when the Earth is believed to have suffered two of its most severe
146 periods of glaciation (Hoffman et al., 1998) and entered into a SB climate
147 state. This period coincided with large carbon dioxide fluctuations, while
148 the solar constant (about 1365 Wm⁻² in present conditions) is believed to
149 have been 94 % of current levels, rising to 95% by the end of the Neopro-
150 terozoic (Gough, 1981; Pierrehumbert et al., 2011). The two main factors
151 effecting concentration of atmospheric CO₂ are biotic activity and volcanism.
152 Volcanic eruptions bring about very sudden and dramatic increases in CO₂
153 concentration. This process provides a potential mechanism through which
154 the climate state can exit the SB condition, by increasing the opacity of
155 the atmosphere and enhancing the greenhouse effect. The biospheric effect
156 tends to occur more gradually as the biotic activity and atmospheric com-
157 position are coupled so that large fluctuations of the carbon pools take place
158 over large time scales. Note that the effect of SB events on the biosphere
159 is believed to have been disastrous. Carbon-isotope ratios characteristic of
160 Earths mantle (Hoffman et al., 1998; Kennedy et al., 1998) rather than of life
161 processes recorded immediately below and above the glacial deposits imply
162 that oceanic photosynthesis was effectively non-existent during SB events.
163 The result of this and anoxic conditions beneath the ice should have lead to
164 the disappearance of most kinds of forms of life except bacteria. The final
165 disappearance of SB conditions since the Neoproterozoic may have been the
166 main contributing factor in the development of complex multi-cellular life
167 that began around 565 million years ago.

168 Based on the evidence supported by (Hoffman et al., 1998; Hoffman and
169 Schrag, 2002), it is therefore expected that the Earth is potentially capable
170 of supporting multiple steady states for the same values of some parameters
171 such as the solar constant and the concentration of carbon dioxide, which
172 directly affect the radiative forcing. It is important therefore to explore this
173 hypothesis, due to the relevance for the history of our planet but also to
174 help understand other planets capability for supporting life. Initial research
175 using simple 0-D models (Budyko, 1969; Sellers, 1969), 1-D models (Ghil,
176 1976) as well as more recent analyses performed using complex 3-D gen-
177 eral circulation models (Marotzke and Botztet, 2007; Voigt and Marotzke,
178 2011; Pierrehumbert et al., 2011), provide support for the existence of such

179 bistability. The SB→W and W→SB transitions tend to occur in an abrupt
180 rather than a smooth transition. The main mechanism triggering such abrupt
181 transitions is the positive ice-albedo feedback (Budyko, 1969; Sellers, 1969).
182 Such a feedback is associated with the fact that as temperatures increase, the
183 extent of snow and ice cover decreases thus reducing the albedo and there-
184 fore increasing the amount of sunlight absorbed by the Earth system. Con-
185 versely, a negative fluctuation in the temperature leads to an increase in the
186 albedo therefore reinforcing the cooling. The presence of such catastrophic
187 climate shifts (Arnol'd, 1992) suggest the existence of a global bifurcation
188 in the climate system for certain combinations of its descriptive parameters
189 (Fraedrich, 1979). The loss of stability realized in the W→SB and SB→W
190 transitions is related to the catastrophic disappearance of one of the two
191 attractors describing the two possible climatic states, as a result of a set of
192 complicated bifurcations.

193 Starting from present conditions, the most obvious physical parameters
194 to modulate in order to bring about the transition to the SB state is the solar
195 constant. Even if other model experiments (Voigt and Marotzke, 2011) show
196 that the decrease in CO₂ alone can bring about transition to the SB state,
197 this requires approximately an 80% decrease in CO₂ concentration, compared
198 to a decrease of less than 10% for the solar luminosity. The Neoproterozoic
199 however highlights the importance of considering the changes in the CO₂
200 levels as a mechanism for the transitions to and from the SB climate state,
201 and therefore the dramatic impact it can have on the overall state of the
202 climate system. It is therefore interesting to alter both the solar luminosity
203 and the atmospheric opacity as these are two important parameters affecting
204 the overall properties of the system. If one wants to explore extensively the
205 parametric space of climate steady states, it is therefore necessary to consider
206 a wide range of values for both of these parameters.

207 Using PlaSim, a general circulation model of intermediate complexity
208 (Fraedrich et al., 2005), we study the climate states realised when the solar
209 constant is modulated between 1160 Wm⁻² and 1510 Wm⁻² and the values
210 of [CO₂] are varied between 90 to 2880 ppm. Our aim here is an empiri-
211 cal (i.e. based on model simulations) reconstruction of the global structural
212 properties of the climatic attractors. For both W and SB states we com-
213 pute surface temperature, material entropy production, meridional energy
214 transport, Carnot efficiency (Johnson, 1997) and dissipation of kinetic en-
215 ergy and propose empirical relationships in the parametric plane (S^* , [CO₂]).
216 We will look for an empirical relation for the two transition lines (W→SB

and SB→W) in the parametric plane between S^* and the natural logarithm of $[\text{CO}_2]$ which marks the boundaries of the hysteresis in the climate system. The aforementioned quantities are used to explain changes in large-scale climate behaviour and the effect of climate change on features such as stratification and baroclinicity in order to understand changes in the meridional heat transport across the parameter range. It will also be shown that the Carnot efficiency has a key role in defining the stability of the system which is related to abrupt climatic shifts.

The paper is structured in the following way: in Section 2 we describe details of the non-equilibrium thermodynamics of the climate and the diagnostic tools used. Section 3 is dedicated to the description of the PlaSim climate model and of the experimental setup. In Section 4 we discuss the results of the simulations, in Section 5 we propose parametrisations of the main non-equilibrium properties of the system as a function of the mean surface temperature or emission temperature, and in Section 6 we present our conclusions.

2. Non-equilibrium Thermodynamics of the climate

In this section we recapitulate some thermodynamic properties of the climate system and introduce the notation used throughout this chapter. We follow what presented in Lucarini (2009). If the climate system is encompassed by a domain Ω , the total energy budget is given by $E(\Omega) = P(\Omega) + K(\Omega)$, where K represents the total kinetic energy and P is the moist static potential energy, which includes contributions from the thermal (including latent heat) and potential energy. The time derivative of K and P can be found to be $\dot{K} = -D + W$ and $\dot{P} = \dot{\Psi} + D - W$, where D is the dissipation and therefore always positive, W is the instantaneous work done by the system and $\dot{\Psi}$ which is the heating due to convergence of turbulent heat fluxes and radiative heat, such that $\dot{E} = \dot{\Psi}$. The dependence on Ω has been dropped for convenience. As soon as the climate is considered as a non-equilibrium steady state system (NESS, see Gallavotti (2006)), we have that over long time scales $\bar{\dot{E}} = \bar{\dot{P}} = \bar{\dot{K}} = 0$ (the bar indicates averaging over long time periods). Let us define \dot{Q} as the local heating rate so that $\dot{Q} = \rho(\epsilon^2 - \nabla \cdot H)$ (Lucarini, 2009) where $\epsilon^2 > 0$ is the local rate of heating due to viscous dissipation of kinetic energy and H is given by the sum of turbulent heat fluxes plus radiative energy fluxes. We split the domain Ω into the domain Ω^+ , where $\dot{Q} = \dot{Q}^+ > 0$, and Ω^- in which $\dot{Q} = \dot{Q}^+ < 0$.

253 Therefore, we find that \dot{Q}^+ and \dot{Q}^- integrated over Ω equal the derivative of
 254 the total heating due to dissipation, D and the convergence of heat fluxes $\dot{\Psi}$:

$$\dot{\Psi} + D = \dot{P} + W = \int_{\Omega^+} dV \rho Q^+ + \int_{\Omega^-} dV \rho Q^- = \dot{\Phi}^+ + \dot{\Phi}^- = \dot{\Phi} \quad (1)$$

255 Where the quantities $\dot{\Phi}^+$ and $\dot{\Phi}^-$ are positive and negative at all times,
 256 respectively. Since dissipation is positive definite, $-\overline{\dot{K}} + \overline{\dot{W}} = \overline{\dot{D}} = \overline{\dot{P}} + \overline{\dot{W}} =$
 257 $\overline{\dot{W}} = \overline{\dot{\Phi}^+} + \overline{\dot{\Phi}^-} > 0$. On spatial scales far smaller than Ω itself, it is practical
 258 to assume local equilibrium (local thermodynamic equilibrium hypothesis,
 259 DeGroot and Mazur (1984)) so that locally $\dot{Q} = \dot{s}T$ with \dot{s} the time derivative
 260 of the entropy density. The total rate of change of the entropy of the system
 261 is:

$$\dot{S} = \int_{\Omega^+} dV \rho \dot{Q}^+ / T + \int_{\Omega^-} dV \rho \dot{Q}^- / T = \int_{\Omega^+} dV \rho |\dot{s}^+| + \int_{\Omega^-} dV \rho |\dot{s}^-| = \dot{\Sigma}^+ + \dot{\Sigma}^- \quad (2)$$

262 where $\dot{\Sigma}^+ > 0$ and $\dot{\Sigma}^- < 0$. Using equation (2) and assuming that the
 263 Earth system is in a steady state, over a long time average, $\overline{\dot{\Sigma}^+} = -\overline{\dot{\Sigma}^-}$ as
 264 $\overline{\dot{S}} = 0$. Therefore, $2\overline{\dot{\Sigma}^+} = \overline{\int_{\Omega} dV \rho |\dot{s}|}$, so that $\overline{\dot{\Sigma}^+}$ measures the absolute value
 265 of the entropy fluctuations throughout the domain. When integrating over
 266 the whole domain and considering long time average, we have the follow-
 267 ing equivalent expressions for the thermodynamic quantities: $\overline{\dot{\Phi}^+} = \overline{\dot{\Sigma}^+} \overline{\Theta^+}$
 268 and $\overline{\dot{\Phi}^-} = \overline{\dot{\Sigma}^-} \overline{\Theta^-}$, where $\overline{\Theta^+}$ and $\overline{\Theta^-}$ are the time and space averaged tem-
 269 peratures of the Ω^+ and Ω^- domains respectively. Since $|\overline{\dot{\Sigma}^+}| = |\overline{\dot{\Sigma}^-}|$ and
 270 $|\overline{\Phi^+}| > |\overline{\Phi^-}|$, it can be shown that $\overline{\Theta^+} > \overline{\Theta^-}$, i.e absorption typically occurs
 271 at higher temperature than release of heat (Peixoto et al., 1991; Johnson,
 272 1997). The work done by the Carnot engine of the climate system is found
 273 to be, $\overline{\dot{W}} = \eta \overline{\dot{\Phi}^+}$, where

$$\eta = \frac{\overline{\dot{\Phi}^+} + \overline{\dot{\Phi}^-}}{\overline{\dot{\Phi}^+}} \quad (3)$$

274 can be defined as the Carnot efficiency of the system. As shown in Lorenz
 275 Lorenz (1967) and clarified in Johnson (1997) (2000) the long term average
 276 of the work performed by the system is equal to the long-term average of the
 277 generation of available potential energy, as typical of forced-dissipative steady

278 states. The Earth exists in a steady state maintained far from equilibrium
 279 by net radiative heating in the warm region (low latitude in our planet) and
 280 net cooling at the cold regions (high latitude in our planet), which are com-
 281 pensated by large scale transports performed by the planetary atmpsphere.
 282 This gives rise to ongoing irreversible processes, including phase transitions
 283 (H₂O in the case of our planet) and frictional dissipation, which are charac-
 284 terized by a positive entropy production. The entropy production due to the
 285 irreversibility of the processes occurring within the climatic fluid is called the
 286 material entropy production, \dot{S}_{mat} and can be written in general terms as:

$$\overline{\dot{S}_{mat}} = \overline{\int_{\Omega} \frac{\epsilon^2}{T} dV} + \overline{\int_{\Omega} \vec{F}_{SH} \cdot \nabla \frac{1}{T} dV} + \overline{\int_{\Omega} \vec{F}_{LH} \cdot \nabla \frac{1}{T} dV} \quad (4)$$

287 where the first, second, and third terms on the RHS are related to the dis-
 288 sipation of kinetic energy, and to the transport of sensible and latent heat
 289 respectively. We now wish to link the terms of the entropy budget in eq. (2)
 290 with those of the entropy production in eq. (4). The second law of ther-
 291 modynamics states that the entropy variation of a system at temperature T
 292 receiving an amount of heat δQ is larger than or of equal to $\delta Q/T$ Landau
 293 and Lifshitz (1980). In this case:

$$\begin{aligned} \overline{\dot{S}_{mat}(\Omega)} &\geq \overline{\dot{S}_{min}(\Omega)} = \overline{\left(\frac{\int_{\Omega} dV \rho \dot{Q}}{\int_{\Omega} dV \rho T} \right)} = \overline{\left(\frac{\Phi^+ + \Phi^-}{\langle \Theta \rangle} \right)} \approx \\ 294 &\approx \frac{\overline{\Phi^+} + \overline{\Phi^-}}{\langle \Theta \rangle} \approx \frac{\overline{\Phi^+} + \overline{\Phi^-}}{\frac{(\Theta^+ + \Theta^-)}{2}} = \frac{\overline{W}}{\frac{(\Theta^+ + \Theta^-)}{2}} \end{aligned} \quad (5)$$

295 where $\overline{\dot{S}_{mat}(\Omega)}$ is the long-term average of the material entropy production,
 296 $\overline{\dot{S}_{min}(\Omega)}$ is its lower bound, i.e. the minimal value of the entropy produc-
 297 tion compatible with the presence of a Lorenz energy cycle with average
 298 intensity W ?? and $\langle \Theta \rangle$ is the density averaged temperature of the system.
 299 The approximation holds as long as we can neglect the impact of the cross-
 300 correlation between the total net heat balance and the average temperature
 301 and we can assume that $\langle \Theta \rangle$ can be approximated by the mean of the two
 302 Carnot temperatures Θ^+ and Θ^- . We can explicitly write $\dot{S}_{min}(\Omega)$ as:

$$\overline{\dot{S}_{min}(\Omega)} \approx \frac{\overline{W}}{(\Theta^+ + \Theta^-)/2} = \frac{\eta \overline{\Phi^+}}{(\Theta^+ + \Theta^-)/2} =$$

303

$$= \eta \frac{\Theta^+}{(\Theta^+ + \Theta^-)/2} \overline{\dot{\Sigma}^+} = \frac{\eta}{1 - \eta/2} \overline{\dot{\Sigma}^+} \approx \eta \overline{\dot{\Sigma}^+} \quad (6)$$

304 where the last approximation holds as long as $\eta \ll 1$, which is typically
 305 the case. Therefore, η sets also the proportionality factor relating the lower
 306 bound to the entropy production of the system $\overline{\dot{S}_{min}(\Omega)}$ due to macroscopi-
 307 cally irreversible processes to the absolute value of the entropy fluctuations
 308 inside the system due to macroscopically reversible heating or cooling pro-
 309 cesses. Note that if the system is isothermal and at equilibrium the internal
 310 entropy production is zero, since $\eta \rightarrow 0$. The lower bound to the material
 311 entropy production corresponds to the contribution coming from the dissi-
 312 pation of kinetic energy through viscous processes. Therefore, the average
 313 material entropy production can be expressed as $\overline{\dot{S}_{mat}} = \overline{\dot{S}_{min}} + \overline{\dot{S}_{exc}}$, where
 314 $\overline{\dot{S}_{exc}}$ is the excess of entropy production with respect to the minimum, which
 315 results from the heat transport down the temperature gradient ((Lucarini,
 316 2009)). We can define:

$$\alpha \approx \frac{\overline{\dot{S}_{exc}}}{\overline{\dot{S}_{min}}} \approx \frac{\int_{\Omega} dV (\overline{\vec{F}_{SH} + \vec{F}_{LH}}) \cdot \nabla(\frac{1}{T})}{(\overline{W}/\langle\Theta\rangle)} \geq 0 \quad (7)$$

317 as a parameter of the irreversibility of the system, which is zero if all the
 318 production of entropy is due to the unavoidable viscous dissipation of the
 319 mechanical energy. As $\overline{\dot{S}_{mat}} \approx \eta \overline{\dot{\Sigma}^+} (1 + \alpha)$, we have that the entropy pro-
 320 duction is maximized if we have a joint optimization of heat transport and
 321 the production of mechanical work. Note that, if heat transport down the
 322 temperature gradient is very strong, the efficiency η is small because the dif-
 323 ference between the temperatures of the warm and cold reservoirs is greatly
 324 reduced (the system is almost isothermal), whereas, if the transport is very
 325 weak, the factor α is small. The parameter α introduced above is related to
 326 the Bejan number \mathcal{Be} as $\mathcal{Be} = \alpha + 1$ (Paoletti et al., 1989).

327 3. Experimental setup

328 We study dynamical and thermodynamical properties of the Earths cli-
 329 mate using the PlaSim climate model. This is motivated by the fact that
 330 our study requires altering very extensively some parameters of the climate
 331 system and producing many simulations. Therefore we need a model which
 332 is flexible and fast to run rather than a state-of-the-art model encompassing

333 as many processes occurring in the Earth as possible. PlaSim (Fraedrich
 334 et al., 2005) is a climate model of intermediate complexity, freely avail-
 335 able at <http://www.mi.uni-hamburg.de/plasim>. Its dynamical core is for-
 336 mulated using the primitive equations for vorticity, divergence, temperature
 337 and the logarithm of surface pressure, solved using the spectral transform
 338 method (Eliassen et al., 1970; Orszag, 1970). Unresolved processes for long
 339 (Sasamori, 1968) and short (Lacis and Hansen, 1974) wave radiation, shal-
 340 low, moist (Kuo, 1965, 1974) and dry convection, cloud formation (Stephens,
 341 1978; Stephens et al., 1982; Slingo and Slingo, 1991) and large scale precipi-
 342 tation, latent and sensible heat boundary layer fluxes, horizontal and vertical
 343 diffusion (Louis, 1979; Louis et al., 1981; Laursen and Eliassen, 1989) are pa-
 344 rameterized. The model is coupled to a 50-*m* deep mixed layer ocean which
 345 contains a thermodynamic sea-ice model. The advantage of using a slab
 346 ocean as opposed to a full ocean is that it allows for the climate system to
 347 reach a steady state in less than 35 years after a change in e.g. the solar con-
 348 stant. With full ocean coupling, the integration time of the model and the
 349 time needed to reach a steady state would be an order of magnitude larger
 350 (Voigt and Marotzke, 2011). We wish to emphasize that whereas most state-
 351 of-the-art general circulation models feature considerable energy imbalances,
 352 as highlighted by Lucarini et al. (2011), the energy bias is of the order of
 353 0.5 Wm^{-2} in very extreme climate conductions and less than that for more
 354 usual choices of climatic parameters. Moreover a tested entropy diagnostic
 355 is available (Fraedrich and Lunkeit, 2008), thus making it well suited for this
 356 work. The model is run at T21 resolution (approximately $5.6^\circ \times 5.6^\circ$) with
 357 10 vertical levels. Changing S^* over a wide range of $[\text{CO}_2]$ of 90, 180, 270,
 358 360, 540, 720, 1080, 1440, 2160 and 2880 ppm, we are able to reconstruct the
 359 SB and W climate states. The procedure occurs as follows for each of the
 360 considered values of $[\text{CO}_2]$:

- 361 1. the model is run to a W steady state for 100 years with S^* equal to
 362 1510 Wm^{-2} ;
- 363 2. S^* is decreased by a small amount for each value of CO_2 and the model
 364 run is continued until a steady state is reached;
- 365 3. step 2 is repeated until S^* is reduced to 1165 Wm^{-2} ; the point of
 366 $\text{W} \rightarrow \text{SB}$ transition is noted down;
- 367 4. the reverse operation is then performed with S^* increased step by step,

up to the value of 1510 Wm^{-2} , each time allowing the system to reach a steady state; the point of SB→W transition is noted down.

Further to this, we identify the position of the transition to a higher resolution than the rest of the parameter range in the direction of S^* . For values of S^* within 10 Wm^{-2} before the transition, S^* is decreased in intervals of 1 Wm^{-2} , each time permitting 50 years for the system to reach a steady state, until after the transition is observed.

4. Hysteresis, bistability and regime boundaries in a parametric space

4.1. Temperature and entropy production

Initially, the focus is put on analysing the parametric plane ($[\text{CO}_2]$, S^*), which in the following shall be referred to as the CS space, as a function of global mean surface temperature, T_s . The transition zones between the main climate states are clearly defined from the temperature profile. Note, the qualitative properties of the climate system in the CS space, namely the presence of bistability or of just one of the SB/W states, can be reconstructed from any observable of the climate state, but it is most instructive to select first the surface temperature because it is also practically the most relevant. The temperature profile through the CS space is illustrated in Figures 2(a) and 2(b). We can identify two main climatic regimes, observed as two distinct manifolds ($[\text{CO}_2]$, S^* , T_s) and characterized by a sharp change in the profile of T_s when jumping from one manifold to another. We refer to these as the upper and lower manifolds, representative of the W and SB regimes respectively. As would be expected, there is a monotonic increase of temperature with increasing CO_2 or S^* on both manifolds Voigt and Marotzke (2011); Pierrehumbert (2005). The temperature range on the SB and W manifolds are 212 K-242 K, and 254 K-326 K respectively, over the parametric space. We see that the temperature range 242 K-254 K is not permitted by the climate system. Note, due to the different temperature ranges the colour scaling of figures 1(a) and 1(b) is a factor of 4 different, with both scales starting from the same lowest value.

The temperature range of the bistable region in the SB and W regimes are 218 K-242 K and 254 K-300 K respectively, meaning that the rate of change of surface temperature over the same range of S^* and $[\text{CO}_2]$ is approximately twice as large in the W regime with respect to the SB regime, and that the

403 surface temperature difference between the two manifolds ranges between 40
 404 K and 60 K for identical values of S^* and $[CO_2]$. The W states (upper man-
 405 ifold) exists only in the region of the CS space above the W→SB transition
 406 line (the position of this line is expressed as $S^* = S_{sbw}^*$) whereas the SB
 407 states (lower manifold) only in the CS region below the SB→W transition
 408 line (the position of this line is expresses as $S = S_{wsb}^*$). Such lines, which
 409 are well separated and approximately parallel, are illustrated as solid and
 410 dashed purple dashed lines on figures 1(a)-8(b) and have been found within
 411 an accuracy of 2 Wm^{-2} of the solar constant. The solid purple lines indicate
 412 the active transition, dependant on which manifold the climate system lies in
 413 at that moment i.e the active transition for the SB and W states are SB→W
 414 and W→SB respectively. The dashed lines illustrate the location of the inac-
 415 tive transition, when the climate system exists in the alternative state. The
 416 bistable region is therefore located between the dashed and solid purple lines.
 417 As a result, a property of the system is that regardless of which combination
 418 of $[CO_2]$ and S^* is used, the transition from one state to another always
 419 occurs at almost exactly the same temperature. This indicates that the cli-
 420 mate system is “blind” to the mechanism of forcing. The position of the two
 421 boundaries can be parameterised in terms of S^* and CO_2 concentration as:

$$S_{sbw}^* = a_{sbw} \log_{10}[CO_2] + C_{sbw}, \quad S_{wsb}^* = a_{wsb} \log_{10}[CO_2] + C_{wsb} \quad (8)$$

422 where $a_{sbw} \approx a_{wsb} \approx -70 \text{ Wm}^{-2}$, $C_{sbw} \approx 1630 \text{ Wm}^{-2}$ and $C_{wsb} \approx 1440 \text{ Wm}^{-2}$
 423 for the transition SB→W and W→SB respectively and $[CO_2]$ is expressed in
 424 ppm. The size of the bistable region, which we define as B , along S^* can
 425 therefore be defined by the difference between C_{sbw} and C_{wsb} :

$$B = C_{sbw} - C_{wsb}. \quad (9)$$

426 It is found that B is approximately 200 Wm^{-2} . The displacement between
 427 the position of the boundaries gives a precise measure of the hysteretic prop-
 428 erties of the climate (Budyko, 1969; Sellers, 1969; Voigt and Marotzke, 2011;
 429 Lucarini et al., 2010b) since it indicates the size of the overlap between the
 430 two manifolds in the CS plane. The presence of a bistable region implies that
 431 when we change the values of S^* and $[CO_2]$ from an initial to a final value,
 432 the final steady state depends on the initial steady state and on the path of
 433 change of S^* and $[CO_2]$. Let us assume that we start from an initial point
 434 $(S_0^*, [CO_2]_0)$ in the bistable region and in the W state. Let us also assume
 435 we perform a close path of variation of S^* and $[CO_2]$ so that $S_0^* = S_f^*$ and

436 $[CO_2]_0 = [CO_2]_f$. If the path does not cross S_{wsb}^* the final state will be
 437 identical to the initial one, that is, in a time-averaged sense:

$$T_s(S_0^*, [CO_2]_0) = T_s(S_f^*, [CO_2]_f). \quad (10)$$

438 On the other hand, if the closed path crosses the transition line to the second
 439 manifold, the final state will be different from the initial:

$$T_s(S_0^*, [CO_2]_0) \neq T_s(S_f^*, [CO_2]_f). \quad (11)$$

440 If, furthermore, the closed path crosses first S_{wsb}^* and then S_{sbw}^* , then again
 441 $T_s(S_0^*, [CO_2]_0) = T_s(S_f^*, [CO_2]_f)$, since the system has performed first a
 442 W→SB, and then a SB→W transition. The same applies starting from a
 443 SB state and exchanging SB with W in the previous discussion. This is true
 444 for any climate diagnostic. More specifically, in the case of T_s , for W→SB
 445 and SB→W transitions,

$$T_s(S_0^*, [CO_2]_0) > T_s(S_f^*, [CO_2]_f) \quad \text{and} \quad T_s(S_0^*, [CO_2]_0) < T_s(S_f^*, [CO_2]_f) \quad (12)$$

446 respectively. Note that for $S^* > 1440 \text{ Wm}^{-2}$, even if CO_2 is 0 ppm, no
 447 transition to SB state can occur.

448 Figures 3(a) and 3(b) show the reconstruction for the material entropy
 449 production, \dot{S}_{mat} in CS space, computed directly as described in Fraedrich
 450 and Lunkeit (2008). As with temperature, \dot{S}_{mat} increases monotonically with
 451 increasing S^* and $[CO_2]$ on both manifolds. In the SB state, the entropy is
 452 mostly generated by dissipation of kinetic energy and by irreversible sensible
 453 heat transport, because the planet is almost entirely dry. For the W manifold
 454 the main contribution to entropy production comes from latent heat due to
 455 large scale and convective precipitation . In the bistable region, the range of
 456 \dot{S}_{mat} is $(10, 19) 10^{-3} \text{W m}^{-2} \text{K}^{-1}$ and $(34, 62) 10^{-3} \text{W m}^{-2} \text{K}^{-1}$ for the SB and
 457 W respectively, therefore a factor of 3 larger in the W regime with respect
 458 to the SB regime. This confirms that \dot{S}_{mat} may be a better indicator than
 459 temperature for discriminating the SB and W states as already discussed in
 460 Lucarini et al. (2010b). Again, there is a range of values of \dot{S}_{mat} – from 19
 461 to 34 $10^{-3} \text{W m}^{-2} \text{K}^{-1}$ – which is not allowed by the system.

462 In the bistable region, the SB and W states are quantitatively very differ-
 463 ent with respect to their physical properties. The two disjoint attractors can
 464 be thus thought to represent two different worlds, with completely different
 465 dynamical and thermodynamical properties. Therefore we treat them sepa-
 466 rately and then describe how the system makes a transition between them.

467 For this reason in the following two sub-sections dynamical and thermody-
 468 namical properties of the manifolds will be analysed individually in terms of
 469 the vertical and horizontal surface temperature differences, Carnot efficiency,
 470 meridional heat transport and dissipation of kinetic energy. Furthermore we
 471 shall relate these properties to the average mean global temperature and the
 472 material entropy production. As is illustrated as solid and dashed purple
 473 lines, in the CS space figures, each manifold will be divided up in to two sub
 474 regions: W, W/Bistable, on the upper manifold and SB, SB/Bistable on the
 475 lower. Then in a third section, we will analyse the transitions between the
 476 two manifolds occurring in bifurcations regions.

477 4.2. The warm state

478 The meridional energy transport profile is worked out, as explained in Lu-
 479 carini et al. (2011), by integrating over latitude the longitudinally averaged
 480 TOA radiation budget. We then define as a scalar indicator of the transport
 481 half of the sum of the peak values of the poleward heat transport in the two
 482 hemispheres, *MET*. In a moist atmosphere, the average global temperature
 483 and the meridional surface temperature difference, defined in our case as the
 484 difference between the mean surface temperature of the tropical (30S,30N)
 485 and the polar (90S,60S) and (60N,90N) regions (see Figure 5(a)), are the
 486 main contributing factors for controlling the meridional heat transport (see
 487 Figure 4(a)). This is due to the fact that temperature controls the latent
 488 heat released in the atmosphere because of the Clausius-Clapeyron effect
 489 (Held and Soden, 2006) and the meridional temperature gradient controls
 490 baroclinicity of the atmosphere (Stone, 1978). Additionally, another mod-
 491 ulating factor is the vertical stratification of the atmosphere, as conditions
 492 of low stratification in the midlatitudes support stronger baroclinic activity
 493 for a given meridional temperature gradient (Holton, 2004). In the bistable
 494 region of the warm sector meridional heat transport has a flat response to
 495 increasing S^* and $[CO_2]$ and therefore T_s . With increased T_s , water vapour
 496 concentration of the atmosphere increases, thus leading to the strengthening
 497 of the poleward latent heat fluxes. In addition, the increased T_s causes sea
 498 and continental ice as well as seasonal snow cover to retreat towards the
 499 poles, thus lowering the surface albedo gradient. This contributes negatively
 500 to the changes in the meridional transport, because it leads to a decrease in
 501 the baroclinicity.

502 In the W regime, the boundary between the bistable and the monostable
 503 regime approximately marks the point at which the Earth surface loses its

504 permanent sea-ice cover, thus supporting the idea that the presence of bista-
 505 bility is intimately linked with the powerful ice-albedo feedback. For T_s larger
 506 than approximately 300 K, the meridional temperature gradient decreases at
 507 a far slower rate with increasing T_s . This essentially means that in this re-
 508 gion the meridional heat transport is controlled only by the availability of
 509 water vapour in the atmosphere. Therefore at temperatures above 300K, the
 510 meridional heat transport becomes decoupled from the surface meridional
 511 temperature difference. This analysis consequently shows how important the
 512 involvement of the hydrological cycle is in the magnitude of the meridional
 513 heat transport and moreover, it indicates that when going from warm to very
 514 warm climates the hydrological cycle becomes the dominant climatic feature,
 515 leading to strong positive dependence of the meridional heat transport on the
 516 surface temperature. Our results agree with the findings of Caballero and
 517 Langen (2005), who found in aqua planet simulations, that there is little
 518 scope for reducing the meridional temperature gradient further once the sea-
 519 ice and snow have melted. For a constant meridional temperature gradient,
 520 an increase in the meridional latent heat fluxes with increasing global mean
 521 temperature was shown.

522 The conclusions drawn above find further support when looking at the
 523 mid-latitudes vertical temperature difference, ΔT_v , defined as the mean tem-
 524 perature difference between the surface and the 500 hPa level (see Figure
 525 5(b)) and which provides a rough measure of the stratification of the atmo-
 526 sphere of the atmosphere in the baroclinically active regime. The vertical
 527 temperature difference is largest along a band of the CS space centered half
 528 way through the bistable region in the direction of S^* . Our current climate
 529 conditions would appear to be positioned at the centre of the band peak
 530 where such temperature difference peaks, implying conditions of reduced
 531 vertical stratification. For climates colder than present, increasing surface
 532 temperature causes the melting of sea-ice and of seasonal snow cover, so that
 533 the ensuing decrease in surface albedo (leading to increased surface absorp-
 534 tion) accounts for the increasing vertical temperature difference. Instead, in
 535 climates colder than present, the decrease in equatorial vertical temperature
 536 difference with T_s can be understood in terms of increased moist convection
 537 from warmer surface temperatures, resulting in an increase of moisture fluxes
 538 to the upper atmosphere, which then condense and release latent heat. In
 539 the bistable region, for the reasons discussed above, we expect to find a pro-
 540 nounced weakening of the dynamics of the climate system with increasing
 541 surface temperature. We test this hypothesis by computing the strength of

542 the Lorenz energy cycle (Fig. 4(b)), which is equal to the average rate of dis-
 543 sipation of kinetic energy, and the Carnot efficiency of the system (Fig. 6(a)),
 544 which measures, instead, how far from equilibrium the system is. The dis-
 545 sipation, similarly to the meridional temperature gradient, decreases mono-
 546 tonically with the surface temperature, and reaches its largest value just at
 547 the cold boundary of the W manifold. The efficiency is maximized along a
 548 band of climate states characterised by slightly higher temperatures. This
 549 region in the CS space lies about half way between the peak in the merid-
 550 ional and vertical temperature gradients, since a large value of efficiency, by
 551 its very definition, requires a compromises between maximizing these two
 552 gradients. The efficiency decreases monotonically with increasing CO_2 or S^* :
 553 warmer climates are characterised by smaller temperature differences, since
 554 the transport of water vapour acts as a very efficient means for homogenising
 555 the temperature across the system. The system has lower ability to produce
 556 mechanical work and is characterised by very strong irreversible processes,
 557 as described by the very large values of entropy production realised in these
 558 conditions. Consequently the value of the parameter of irreversibility α in-
 559 creases as conditions becomes warmer and warmer (not shown); see also
 560 Lucarini et al. (2010b).

561 4.3. *The snowball state*

562 The SB state is intrinsically simpler than the W state because the hy-
 563 drological cycle has a negligible influence. This is due to the fact that at-
 564 mospheric temperatures are so low that we have in all cases an almost dry
 565 atmosphere. As a result we have, e.g. that, as opposed to the W state,
 566 the parameter α is small (~ 1) and weakly dependent on the value of the
 567 parameter S^* and $[\text{CO}_2]$ (not shown); see also Lucarini et al. (2010b).

568 Moreover, in the SB state the meridional gradients (and not only the
 569 globally averaged values) of albedo are very low and depend weakly on S^*
 570 and the CO_2 , because under all conditions the sea surface is frozen almost
 571 everywhere and the continents are covered by ice and snow. The meridional
 572 heat transport (Figure 7(a)) is much smaller than for the corresponding W
 573 states, because in the SB state a large fraction of the radiation is reflected
 574 back to space and the albedo gradients are small, so that the energy im-
 575 balance between low and high latitudes is small. Throughout the SB state,
 576 increases in S^* and $[\text{CO}_2]$, which lead to an increase in the surface temper-
 577 ature and in the rate of entropy production are accompanied by increases in

578 the meridional heat transport and in the dissipation of kinetic energy (Fig-
 579 ure 7(b)). This tells us that with increased meridional heat transport the
 580 intensity of the circulation also increases. However we find that the merid-
 581 ional temperature difference (not shown) has a very weak dependence on
 582 changing $[\text{CO}_2]$ and S^* , as it varies by only 4 K across the explored param-
 583 eter range, so that the changes in the baroclinicity of the system cannot be
 584 due to changes in the meridional heat transport and in the intensity of the
 585 Lorenz energy cycle. The lack of large variations in the meridional surface
 586 temperature profile are essentially due to the fact that the net input of short-
 587 wave radiation is kept almost fixed by the constant surface albedo and by the
 588 virtue of almost no cloud cover. The system therefore can be seen as rather
 589 rigid, as changes in the absorbed radiation are almost exactly compensated
 590 by changes in the meridional heat transport. The re-equilibration mechanism
 591 must then contain elements which are not present in the classic baroclinic
 592 adjustment (Stone, 1978). We find that the midlatitudes vertical tempera-
 593 ture gradient (Figure 8(b)) increases substantially with increased value of S^*
 594 and $[\text{CO}_2]$, as an effect of the increased absorption of radiation near the sur-
 595 face. The reduced vertical stratification leads to more pronounced baroclinic
 596 activity even for a fixed meridional temperature gradient, thus leading to an
 597 increase in the meridional heat transport and in the intensity of the Lorenz
 598 energy cycle. The argument is in this case quite straightforward because we
 599 are considering an almost dry atmosphere. The efficiency has a dependence
 600 on S^* and $[\text{CO}_2]$ which, as in the W case, is intermediate between those of
 601 the meridional and vertical temperature gradient fields. In the case of the
 602 SB state, the main signature is given by the vertical gradient (Figure 8(b)).
 603 This further reinforces the idea that the investigation of meridional temper-
 604 ature gradients is not enough to grasp the mechanisms through which the
 605 system generates available potential energy and material entropy production
 606 (Lucarini et al., 2011).

607 4.4. *Transition and comparison between manifolds*

608 Up to now, the W and SB states have been characterised as two entirely
 609 distinct climate regimes, and have underlined that the basic mechanisms
 610 of re-equilibration are rather different. In this subsection we would like to
 611 present some ideas aimed at making sense of the transitions between the
 612 two states occurring when we get close to the boundary of the upper or of
 613 the lower manifold. As has been seen, the W→SB transition is associated
 614 to a large decrease of surface temperature, rate of material entropy produc-

tion, and meridional heat transport. This is intimately related to the fact that whereas in the W state the hydrological cycle is a major player of the climate dynamics, in the SB state the hydrological cycle is almost absent. Nonetheless, this does not say much about the processes leading to the transition between the two states, or better, describing how one of the attractors disappears.

We have also discovered that the usual dynamical indicators of the atmospheric state, i.e. the meridional temperature gradient and the vertical stratification do not necessarily indicate whether or not we are close to an irreversible transition of the system, e.g. by signaling something equivalent to a loss of elasticity of the system. In this regard, it is much more informative to observe how the efficiency behaves near the transitions. We find that, as a general rule, each transition is associated to a notable decrease (more than 30%) of the efficiency of the system, and the closer the system gets to the transition in the CS space, the larger is the value of the efficiency. This can be interpreted as follows. If the system approaches a bifurcation point, its positive feedbacks become relatively stronger and the negative feedbacks, which act as re-equilibrating mechanisms, become less efficient. As a result, the differential heating driving the climate is damped less effectively, and the system is further from equilibrium, since larger temperature differences are present. Therefore, the system produces more work, thus featuring an enhanced Lorenz energy cycle and a stronger circulation. At the bifurcation point, the positive feedbacks prevail and the circulation, even if rather strong, is not able to cope with the destabilising processes, and the transition to the other manifold is realised. The new state is, by definition, more stable, and thus closer to equilibrium. The decreased value of the efficiency is exactly the marker of this property. This confirms what has been proposed by Lucarini et al. (2010b) but in much greater generality and can be conjectured to be a rather general properties of non-equilibrium systems featuring structural instabilities.

5. Parameterisations

In the previous sections, we have presented a systematic investigation of the thermodynamical properties of the planet in the SB and W states, obtained by exploring the CS parametric space. As mentioned above, in many cases the main quantity controlling the thermodynamic properties is the average surface temperature T_s only. This statement can be substantiated

by looking at Figs. 2-8 and observing that in most cases the isolines of the depicted thermodynamic quantities are approximately parallel, both in the W and SB state, to the isolines of T_s . This suggests the possibility of establishing approximate empirical laws of the form $\Gamma_{SB}(S^*, [CO_2]) \approx \Gamma_{SB}(T_s(S^*, [CO_2]))$ and $\Gamma_W(S^*, [CO_2]) \approx \Gamma_W(T_s(S^*, [CO_2]))$, where Γ is a thermodynamical property such as, e.g. entropy production, and the lower index refers to whether we are in the SB or W state. For a given Γ , the empirical laws will be in general different in the SB vs in the W state. This result is quite interesting in a classical perspective of climate dynamics, where it is customary to parameterise large scale climate properties as a function of the surface temperature, especially when constructing simple yet meaningful models (Saltzman, 2002).

We want to complement this approach by testing whether it is possible to construct empirical laws expressing the thermodynamical properties of the system as a function of its emission temperature $T_E = (LW_{TOA}/\sigma)^{1/4}$ – where LW_{TOA} is the area- and time-averaged outgoing long wave radiation at the top of the atmosphere and σ the Stefan-Boltzmann constant –, which is a quantity of more readily astrophysical interest and more fundamental physical significance. Therefore, we would like to be able to observe well-defined functions of the form $\Gamma_{SB}(S^*, [CO_2]) \approx \Gamma_{SB}(T_E(S^*, [CO_2]))$ and $\Gamma_W(S^*, [CO_2]) \approx \Gamma_W(T_E(S^*, [CO_2]))$, which, given the observation made above, requires also the existence of an approximate relationship $T_E \approx T_E(T_s)$.

Indeed, Fig. 9 shows that it is possible to observe an empirical, monotonic relationship between T_s and T_E in a vast range of climate states, including both the W and SB states. Obviously, the correspondence between the two variables is not perfect, so that for each value of T_s it is possible to have climates featuring a range of values of T_E , and vice versa. The spread associated with the ensemble points is of order 10 K and 5 K for T_E , and 20 K and 10 K for T_s in the W and SB states respectively. A range of values of T_E (230 – 240 K) and T_s (240 – 260 K) are not permitted by the system as a result of the ice-albedo instability. We can now proceed to see to which extent the quantities T_s and T_E can be used as a good predictor of the thermodynamic properties of the planet and compare their skill with T_s . The following description is, on purpose, purely qualitative, because we mostly want to show to what extent T_E and T_s can be used as predictor, rather than discussing in detail what are the appropriate transfer functions.

Figure 10(a) and 10(b) show that a clear monotonic relationship exists

688 between T_E , T_s and the material entropy production $\overline{\dot{S}_{mat}}$, with higher val-
 689 ues of T_E and T_s associated with larger values of $\overline{\dot{S}_{mat}}$. It is important to
 690 note that while the values of $\overline{\dot{S}_{mat}}$ and T_s are related to a very high degree
 691 of approximation on a one-to-one basis, the functional dependence between
 692 T_E and $\overline{\dot{S}_{mat}}$ is less well defined (the spread of points is much wider than in
 693 the T_s case, and especially so in the very warm regimes). Note also that the
 694 dependences, while monotonic in both cases, are very different between the
 695 W and SB states. The common line is that the more is the energy absorbed
 696 by the planet (larger values of T_E), the more intense in the production of
 697 material entropy. Note that this is indeed not the case when considering the
 698 intensity of the Lorenz energy cycle (Fig. 11(a) and 11(b)): higher absorp-
 699 tion of energy corresponds to a weaker energy cycle in the W state and to
 700 a stronger cycle in the SB state. Therefore, the increase in the entropy pro-
 701 duction with T_E is due, in the SB case, to the increased dissipation of kinetic
 702 energy, while in the W state it is due to the greatly enhanced hydrological
 703 cycle. In agreement with what has been discussed in the previous section, one
 704 can explain the contrasting responses of the W and SB states to increases in
 705 the absorption of energy by analyzing the Carnot efficiency of the planetary
 706 fluid (Fig. 12). It is interesting to note that, at the transitions, the values of
 707 the efficiency are practically equal: $\eta_{W \rightarrow SB} \approx \eta_{SB, W} \approx 0.03$. Moreover, we
 708 observe that η saturates in the very cold regime of SB states and very warm
 709 regime of W (see Fig. 12) at $\eta_{sat, W} \approx \eta_{sat, SB} \approx 0.012$. Also for the Lorenz
 710 energy cycle and the efficiency, T_s does a much better job as predictor of the
 711 thermodynamic quantities, since the spread of points is much higher when
 712 considering T_E .

713 Last, we want to present the link between T_E , T_s and the meridional
 714 energy transport MET (Fig. 13). We observe that in the SB regime there
 715 is a weakly positive relationship between T_E (T_s) and the transport, for the
 716 reasons described in the previous section; instead, for a vast range of values
 717 of T_E (T_s) in the W regime, the transport is almost insensitive to T_E (T_s),
 718 as discussed thoroughly in Caballero and Langen (2005) and Donohoe and
 719 Battisti (2011, 2012). The rigidity of the climate system has been attributed
 720 by Donohoe and Battisti (2011, 2012) to the fact that the meridional heat
 721 transport is mainly determined by planetary albedo and thus atmospheric
 722 composition rather than surface albedo and sea-ice coverage. However, such
 723 a mechanism ceases to exist when the ice albedo feedback becomes ineffective
 724 because of the disappearance of sea ice above a threshold value of $T_E \approx 255$

725 K ($T_s \approx 300$ K). Above this value, we observe a steep monotonic increase of
726 the transport with temperature, because changes in the latent heat transport
727 are mainly responsible for this behavior. This agrees with the idea that the
728 dynamics and sensitivity of a warm planet is, in some sense, dominated by
729 the hydrological cycle. In this latter case, the skill of the two temperature
730 quantities in parameterising the *MHT* is comparable.

731 Figs 10-13 clearly define the transfer functions allowing to compute the
732 thermodynamic properties of the planet from the value of T_E or T_s only:
733 this is definitely intriguing because it paves the way for computing non-
734 equilibrium properties from a quantity describing the zero-order radiation
735 balance of the system at the top of the atmosphere and of the radiative-
736 convective equilibrium at surface (in the case of T_s). Let us finally note that,
737 in general, the functional dependences of the thermodynamic quantities on
738 T_s is more precisely defined than the one on T_E since these show a larger
739 spread of the ensemble points. This is particularly evident in quantities such
740 as \dot{S}_{mat} (Fig. 10) and η (Fig. 12), \overline{W} (Fig. 11) but less in others, e.g. *MET*
741 (Fig. 13). Figures (9-12) leave various open questions which definitely need
742 to be accurately addressed in future studies: i) why is it possible to use
743 to a good degree of approximation the quantity T_E to parameterise the non-
744 equilibrium thermodynamical properties of a system? ii) why does the surface
745 temperature does an even better job (actually, astounding) in controlling such
746 complex properties? iii) is the result on the decrease of the efficiency at the
747 bifurcation points in both $W \rightarrow SB$ and $SB \rightarrow W$ transitions of more general
748 relevance?

749 6. Summary and conclusions

750 Motivated by the recent discoveries of extrasolar planets, in this contribu-
751 tion we have shown that the habitability conditions, for an Earth-like planet,
752 is a necessary but not solely sufficient condition since two stable sets of states
753 are possible, with one of the two characterized by the global glaciation of wa-
754 ter. In particular we have shown how the stability properties of the climate
755 system depend on the modulation of the two main parameters describing
756 the radiative forcing, i.e. the energy input of the parent star and the long
757 wave opacity of the atmosphere. In our analysis we propose that the point of
758 view of non-equilibrium thermodynamics is especially useful for understand-
759 ing the global properties of the climate system and for interpreting its global
760 instabilities.

761 We have discovered that in a rather wide parametric space, which in-
 762 cludes the present climate conditions, the climate is multistable, i.e. there
 763 are two coexisting attractors, one characterised by warm conditions, where
 764 the presence of sea ice and seasonal snow cover is limited (W state), and
 765 one characterised by a completely frozen sea surface, the so-called snowball
 766 (SB) state. Our results, obtained using the climate model PlaSim, confirm
 767 and extend what has been obtained in various studies performed with mod-
 768 els of various degrees of complexity. We point the reader to Pierrehumbert
 769 et al. (2011) and Lucarini et al. (2010b) for an extensive discussion. In this
 770 regard, the main improvement of this work is that a two dimensional para-
 771 metric space is explored (whereas usually variations in the solar constant or
 772 in the opacity of the atmosphere are considered separately), which allows the
 773 gathering of more complete information on the possible states of the climate
 774 system and actual mechanisms relevant in a paleoclimatological context, as
 775 explained in Pierrehumbert et al. (2011). For all considered values of $[\text{CO}_2]$,
 776 which range from 90 to about 3000 ppm, the width of the bistable region is
 777 about 200 Wm^{-2} in terms of the value of the solar constant, and its posi-
 778 tion depends linearly on the logarithm of the $[\text{CO}_2]$, being centered around
 779 smaller values of the solar constant for increasing opacity of the atmosphere,
 780 shifting by about 15 Wm^{-2} per doubling of CO_2 concentration. The W state
 781 is characterized by surface temperature being 40 K-60 K higher than in the
 782 SB state, and also, in terms of the material entropy production, is larger by a
 783 factor of 4 (order of $40 - 60 \cdot 10^{-3} \text{ Wm}^{-2}$ vs. $10 - 15 \cdot 10^{-3} \text{ Wm}^{-2}$). The bound-
 784 aries of the bistable region are approximately isolines of the globally averaged
 785 surface temperature, and in particular, the warm boundary, beyond which
 786 the SB state cannot be realized, is characterized by vanishing permanent
 787 sea ice cover in the W regime. This reinforces the idea that the ice-albedo
 788 feedback is the dominant mechanism for the multistability properties.

789 The thermodynamical and dynamical properties of the two states are
 790 largely different, as if we were discussing two entirely different planets. In
 791 the W state the climate is dominated by the hydrological cycle and latent
 792 heat fluxes are prominent in terms of redistributing the energy in the system
 793 and as contributors to the material entropy production. The SB state is
 794 eminently a dry climate, where heat transport is realized through sensible
 795 heat fluxes and entropy is mostly generated through the dissipation of the
 796 kinetic energy. The dryness of the SB atmospheres also explains why the
 797 climate sensitivity is much smaller.

798 In the bistability region of the W states, the meridional heat transport

799 is rather constant, as the contrasting effect of the enhancement of latent
 800 heat fluxes driven by increasing surface temperature and the reduction in
 801 the baroclinicity due to the decrease in the meridional temperature gradient
 802 compensate almost exactly. In the W state beyond the bistability region,
 803 the meridional heat flux increases quite dramatically with the surface tem-
 804 perature (Fig. 5(a) and 13) since the compensating albedo mechanisms are
 805 shut off as sea ice is completely removed from the surface. In the SB states,
 806 increased incoming radiation or increased $[\text{CO}_2]$ leads to increases in the
 807 meridional heat transport. In this case, the water vapor plays little role,
 808 and, somewhat surprisingly, the meridional temperature difference has also
 809 a rather flat response to the parametric modulation. In this case, the dom-
 810 inant mechanism determining the properties of the meridional heat transfer
 811 is the change in the vertical stratification, which becomes weaker for warmer
 812 climate conditions. This implies that the atmospheric circulation strength-
 813 ens for increasing values of the solar constant and of $[\text{CO}_2]$. In fact, the
 814 Lorenz energy cycle becomes stronger for warmer climate conditions, and
 815 the Carnot-like efficiency of the climate system has an analogous behavior.
 816 The opposite holds for the W state, where the intensity of the Lorenz energy
 817 cycle and the efficiency decrease for warmer conditions, the reason being that
 818 the water vapor becomes more and more efficient in homogenizing the system
 819 and destroying its ability to generate available potential energy.

820 A general property which has been found is that, in both regimes, the
 821 efficiency increases when we get closer to the bifurcation point and at the
 822 bifurcation point the transition to the newly realized stationary state is ac-
 823 companied by a large decrease in the efficiency. This can be framed in a rather
 824 general thermodynamical context: the efficiency gives a measure of how far
 825 from equilibrium the system is. The negative feedbacks tend to counteract
 826 the differential heating due to the sun's insolation pattern, thus leading the
 827 system closer to equilibrium. At the bifurcation point, the negative feedbacks
 828 are overcome by the positive feedbacks, so that the system makes a global
 829 transition to a new state, where, in turn, the negative feedbacks are more
 830 efficient in stabilizing the system.

831 The results discussed in this paper support the adoption of new diag-
 832 nostic tools based on non-equilibrium thermodynamics for analysing the
 833 fundamental properties of planetary atmospheres. The next step in this
 834 direction is a more quantitative understanding of the global relationships
 835 between surface temperature, material entropy production, meridional heat
 836 fluxes and Carnot-like efficiency for the SB and W states and to propose pos-

sible parametrisations for the dynamical and thermodynamical properties of the SB and W states. Another line of research will explore the dependence of these quantities on other fundamental parameters, e.g. the rotation rate and the surface drag, relevant for atmospheres of terrestrial planets. Recent theoretical results suggest that it is possible to derive up to a good degree of approximation the full thermodynamical properties of planetary atmospheres from the coarse observations of radiative fluxes at TOA and surface (Lucarini et al., 2010b). In this work, we have pursued this line of research by proposing well-defined empirical functions allowing for expressing the global non-equilibrium thermodynamical properties of the system in terms of the globally averaged surface temperature and planetary emission temperature only. The skills of such temperature quantities as predictors is fairly good. The reasons why these parameterisations work so well, and why this is especially the case for globally averaged surface temperature definitely require further investigations. These findings fully confirm the results discussed in Lucarini et al. (2010b,a) and generalize them to a much larger variety of climates, explored by changing both the energy input of parent star and the opacity of the atmosphere. These results reinforce the relevance of the globally averaged surface temperature as a meaningful thermodynamical quantity of the climate system, beyond its obvious practical importance. Moreover, they pave the way for the possibility of practically deducing fundamental properties of planets in the habitable zone from a relatively simple observable.

Acknowledgements

This work was supported by the EU-FP7 ERC grant NAMASTE. The authors would like to thank E. T. Cartman, K. Fraedrich, P. Hauschildt, F. Lunkeit and F. Ragone for their comments and insightful discussions.

References

- Arnol'd, 1992. Catastrophy theory, III edition. Springer, Berlin.
- Bonfils, X., coauthors, 2012. The HARPS search for souther extra-solar planets XXXI. the m-dwarf sample. Astronomy and Astrophysics, in press.
- Budyko, M. I., 1969. The effect of solar radiation variations on the climate of the earth. Tellus 21, 611–619.

870 Caballero, R., Langen, P. L., 2005. The dynamic range of poleward energy
871 transport in an atmospheric general circulation model. *Geophys. Res. Lett.*
872 32, L02705, doi:10.1029/2004GL021581.

873 DeGroot, S., Mazur, P., 1984. *Non-equilibrium thermodynamics*. Dover.

874 Donohoe, A., Battisti, D., 2011. Atmospheric and surface contributions to
875 planetary albedo. *J. Clim.* 24, 4402–4418.

876 Donohoe, A., Battisti, D., 2012. What determines meridional heat transport
877 in climate models? *J. Clim.* 25, 3832–3850.

878 Dvorak, R., 2008. *Extrasolar Planets*. Wiley-VHC.

879 Eliassen, E., Machenhauer, B., Rasmussen, E., 1970. On a numerical method
880 for integration of the hydrodynamical equations with a spectral representa-
881 tion of the horizontal fields. Report no. 2, Inst. of Theor. Met., University
882 of Copenhagen.

883 Fraedrich, K., 1979. Catastrophes and resilience of a zero-dimensional climate
884 system with ice-albedo and greenhouse feedback. *Q J R Meteorolog Soc*
885 105, 147–167.

886 Fraedrich, K., Jansen, H., Luksch, U., Kirk, E., Lunkeit, F., 2005. The planet
887 simulator: towards a user friendly model. *Meteorologische Zeitschrift* 14,
888 299–304.

889 Fraedrich, K., Lunkeit, F., 2008. Diagnosing the entropy budget of a climate
890 model. *Tellus A* 60 (5), 921–931.

891 Gallavotti, G., 2006. *Encyclopedia of mathematical physics*. Elsevier, Ch.
892 Nonequilibrium statistical mechanics (stationary): overview, pp. 530–539.

893 Ghil, M., 1976. Climate stability for a sellers-type model. *J Atmos Science*
894 33, 3–20.

895 Gough, D., 1981. Solar interior structure and luminosity variations. *Solar*
896 *Physics* 74, 21–34.

897 Held, I. M., Soden, B. J., 2006. Robust responses of the hydrological cycle
898 to global warming. *Journal of Climate* 19, 5686–5699.

899 Hoffman, P., J., A. J. K. A., Halverson, G. P., Schrag, D. P., 1998. A neo-
900 proterozoic snowball earth. *Science* 281, 1342–1346.

901 Hoffman, P., Schrag, D. P., 2002. The snowball earth hypothesis: testing the
902 limits of global change. *Terra Nova* 14, 129–155.

903 Holton, J., 2004. *An introduction to dynamic meteorology*. Elsevier.

904 Johnson, D., 1997. "General coldness of climate" and the second law: Impli-
905 cations for modelling the earth system. *Journal of Climate* 10, 2826–2846.

906 Kasting, J., 2009. *How to find a habitable planet*. Princeton University Press.

907 Kennedy, M. J., Runnegar, B., Prave, A. R., Hoffman, K. H., Arthur, M. A.,
908 1998. Two or four neoproterozoic glaciations? *Geology* 26, 1059–1063.

909 Kuo, H., 1965. On formation and intensification of tropical cyclones through
910 latent heat release by cumulus convection. *J. Atmos. Sci.* 22, 40–63.

911 Kuo, H., 1974. Further studies of the parametrisation of the influence of
912 cumulus convection on large-scale flow. *J. Atmos. Sci.* 31, 1232–1240.

913 Lacis, A., Hansen, K., 1974. A parametrisation for the absorption of solar
914 radiation in the earth's atmosphere. *J. Atmos. Sci.* 31, 118–133.

915 Landau, L., Lifshitz, E., 1980. *Statistical Physics, Part 1*. Pergamon: Oxford.

916 Laursen, L., Eliassen, E., 1989. On the effect of the damping mechanisms in
917 an atmospheric general circulation model. *Tellus* 41A, 385–400.

918 Li, J., Chylek, P., 2012. Atmospheric entropy. Part I: Climate dissipation
919 structure. *Journal of Climate* 25, 3173–3190.

920 Lorenz, E., 1967. *The nature and theory of the general circulation of the*
921 *atmosphere*. Vol. 218.TP.115. World Meteorological Organization.

922 Louis, J., 1979. A parametric model of vertical eddy fluxes in the atmosphere.
923 *Bound. Layer Meteorol.* 17, 187–202.

924 Louis, J., Tiedke, M., Geleyn, J., 25-27 Nov. 1981. A short history of the
925 PBL parametrisation at ECMWF. *Proceedings of the ECMWF Workshop*
926 *on Planetary Boundary Layer Parametrization*, 59–80.

927 Lucarini, V., 2009. Thermodynamic efficiency and entropy pro-
 928 duction in the climate system. *Physical Review E* 80, 021118,
 929 doi:10.1103/PhysRevE.80.02118.

930 Lucarini, V., Fraedrich, K., F.Lunkeit, 2010a. Thermodynamics of climate
 931 change: generalized sensitivities. *Atmospheric Chemistry and Physics*, sub-
 932 mitted.

933 Lucarini, V., Fraedrich, K., F.Ragone, 2011. New results on the thermody-
 934 namic properties of the climate. *Journal of the Atmospheric Sciences* 68,
 935 2438–2458.

936 Lucarini, V., Fraedrich, K., Lunkeit, F., 2010b. Thermodynamic analysis of
 937 snowball earth hysteresis experiment: efficiency, entropy production and
 938 irreversibility. *Quarterly Journal of Royal Meteorological Society* 136, 1–
 939 11.

940 Lucarini, V., Ragone, F., 2011. Energetics of climate models: net energy
 941 balance and meridional enthalpy transport. *Reviews of Geophysics* 49,
 942 2009RG000323.

943 Marotzke, J., Botzet, M., 2007. Present-day and ice-covered equilibrium
 944 states in a comprehensive climate model. *Geophys. Res. Lett.* 34, L16704,
 945 doi: 10.1029/2006GL028880.

946 Orszag, S., 1970. Transform method for calculation of vector coupled sums.
 947 *J. Atmos. Sci.*, 890–895.

948 Paoletti, S., Rispoli, F., Sciubba, E., 1989. Calculation of exergetic losses in
 949 compact heat exchanger passages. *ASME AES* 10 (2), 21–29.

950 Pascale, S., Gregory, J., Ambaum, M., Tailleux, R., 2011a. Climate entropy
 951 budget of the HadCM3 atmosphere-ocean general circulation model and
 952 FAMOUS, its low-resolution version. *Climate Dynamics* 36 (5-6), 1189–
 953 1206.

954 Pascale, S., Gregory, J., Ambaum, M., Tailleux, R., 2011b. A parametric
 955 sensitivity study of entropy production and kinetic energy dissipation us-
 956 ing the FAMOUS AOGCM. *Climate Dynamics*, doi 10.1007/s00382-011-
 957 0996-2.

- 958 Peixoto, J., Oort, A., de Almeida, M., Tomé, A., 1991. Entropy budget of
959 the atmosphere. *Journal of Geophysical Research* 96, 10981–10988.
- 960 Peixoto, J. P., Oort, A., 1992. *Physics of the Climate*. Springer-Verlag, New
961 York.
- 962 Perryman, M., 2011. *The Exoplanets Handbook*. Cambridge University
963 Press.
- 964 Pierrehumbert, R., 2005. Climate dynamics of a hard snowball earth. *J.*
965 *Geophys. Res.* 110, D01111, DOI:10.1029/2004JD005162.
- 966 Pierrehumbert, R., Abbot, D., Voigt, A., Koll, D., 2011. Climate of neopro-
967 terozoic. *Ann. Rev. Earth Planet Sci.* 39, 417–460.
- 968 Pujol, T., 2003. Eddy heat diffusivity at maximum dissipation in a radiative-
969 convective one-dimensional climate model. *Journal of the Meteorological*
970 *Society of Japan* 81 (2), 305–315.
- 971 Read, P., 2011. Dynamic and circulation regimes of terrestrial planets. *Plan-*
972 *etary and space sciences* 59, 900–914.
- 973 Saeger, S., 2010. *Exoplanets*. University of Arizona.
- 974 Saltzman, B., 2002. *Dynamic Paleoclimatology*. Accademic Press: New York.
- 975 Sasamori, T., 1968. The radiative cooling calculation for application to gen-
976 eral circulation experiments. *J. Appl. Meteorol.* 7, 721–729.
- 977 Sellers, W. D., 1969. A global climate model based on the energy balance of
978 the earth-atmosphere system. *J. Appl. Meteorol.* 8, 392–400.
- 979 Slingo, A., Slingo, J., 1991. Response of the national center for atmospheric
980 research community climate model to improvements in the representation
981 of clouds. *J. Geophys. Res.* 96, 341–357.
- 982 Stephens, G., 1978. Radiation profiles in extended water clouds. II:
983 parametrization schemes. *J. Atmos. Sci.* 35, 2123–2132.
- 984 Stephens, G., Ackermann, S., Smith, E., 1982. A shortwave parametrization
985 scheme. *J. Atmos. Sci.* 41, 687–690.

- 986 Stone, P., 1978. Baroclinic adjustmnets. J. Atmos. Sci. 35, 561–571.
- 987 Voigt, A., Marotzke, J., 2011. The transition from the present-day climate
988 to a modern snowball earth. Climate Dynamics 35, 887–905.

989 **Figures' captions**

- 990 • Figure 1
- 991 (a) Surface temperature and (b) material entropy production for steady
- 992 states obtained for different values of the solar constant S^* . The present
- 993 climate is marked with a black circle, the W states in red and the SB
- 994 states in blue. Adapted from Lucarini et al. (2010b)

- 995 • Figure 2
- 996 Contour plot of surface temperature (K) as a function of S^* and the
- 997 $[\text{CO}_2]$. The lower SB (a) and upper W (b) manifolds are shown. The
- 998 transition SB→W and W→SB are shown by the upper and lower purple
- 999 lines respectively. The blue dots indicate the values of $(S^*, [\text{CO}_2])$ for
- 1000 which simulations have been performed.

- 1001 • Figure 3
- 1002 Contour plot of $\overline{\dot{S}_{mat}}$ ($10^{-3} \text{Wm}^{-2} \text{K}^{-1}$) as a function of S^* and the $[\text{CO}_2]$
- 1003 for the lower SB (a) and upper W (b) manifolds.

- 1004 • Figure 4
- 1005 Contour plot of: (a) meridional energy transport MET (PW, 1 PW=
- 1006 10^{15} W) and (b) average rate of dissipation of kinetic energy \overline{W} (W
- 1007 m^{-2}) as a function of S^* and the $[\text{CO}_2]$ for the W states.

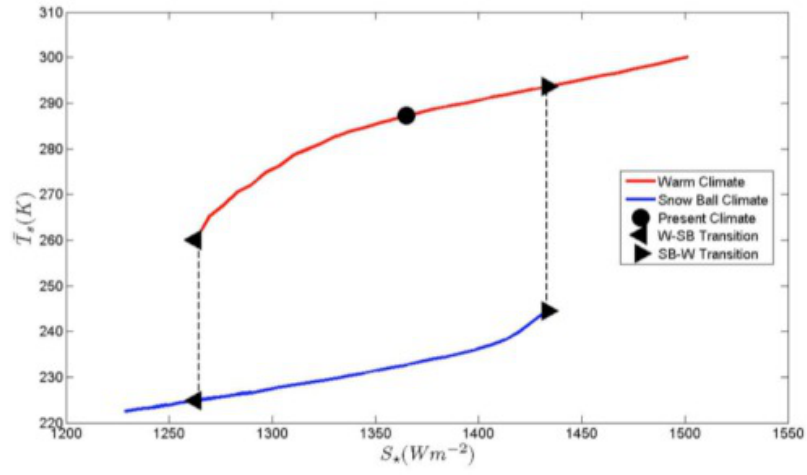
- 1008 • Figure 5
- 1009 Contour plot of: (a) meridional temperature gradient (K) and (b) mid-
- 1010 latitude vertical temperature difference (K) as a function of S^* and the
- 1011 $[\text{CO}_2]$ for the W states.

- 1012 • Figure 6
- 1013 Contour plot of the efficiency as a function of S^* and the CO_2 concen-
- 1014 tration for the W states.

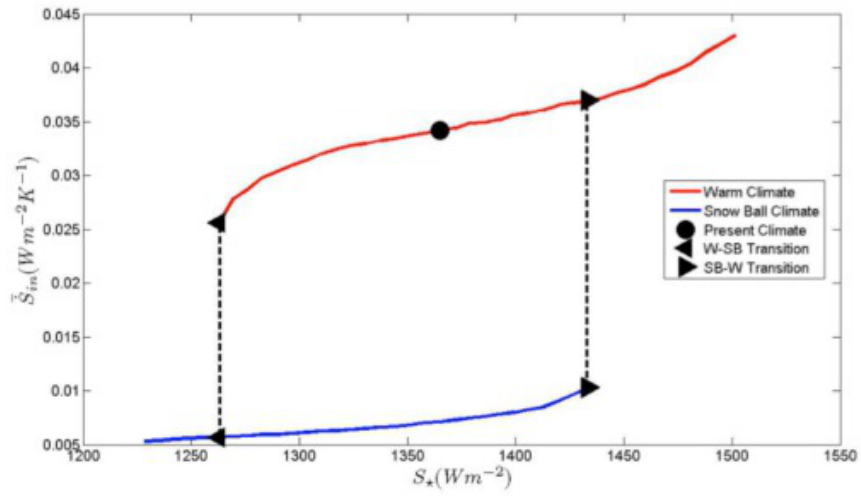
- 1015 • Figure 7
- 1016 Contour plot of: (a) meridional energy transport MET (PW) and (b)
- 1017 average rate of dissipation of kinetic energy (W m^{-2}) as a function of
- 1018 S^* and the $[\text{CO}_2]$ for the SB states

- 1019 • Figure 8
- 1020 Contour plot of (a) the Carnot efficiency η and (b) midlatitude vertical

- 1021 temperature difference (K) as a function of S^* and the $[\text{CO}_2]$ for the
 1022 SB.
- 1023 • Figure 9
 1024 Surface temperature T_s (K) versus emission temperature T_E (K) for the
 1025 W and SB states (each circle represents a simulation). We have marked
 1026 the transitions $W \rightarrow SB$ (red dot – arrow – blue dot) and $SB \rightarrow W$
 1027 (blue dot – arrow – red dot). Same convention is used in Figs. 10-13
 - 1028 • Figure 10
 1029 Material entropy production $\overline{\dot{S}_{mat}}$ ($10^{-3} \text{W m}^{-2} \text{K}^{-1}$) *vs.* (a) emission
 1030 temperature T_E (K) and (b) surface temperature T_s (K).
 - 1031 • Figure 11
 1032 Lorenz Energy cycle strength \overline{W} (W m^{-2}) *vs.* (a) emission temperature
 1033 T_E (K) and (b) surface temperature T_s (K).
 - 1034 • Figure 12
 1035 Carnot efficienct η *vs.* (a) emission temperature T_E (K) and (b) surface
 1036 temperature $T_s(K)$.
 - 1037 • Figure 13
 1038 Meridional heat transport index MET (in PW) *vs.* (a) emission tem-
 1039 perature T_E (K) and (b) surface temperature T_s (K).

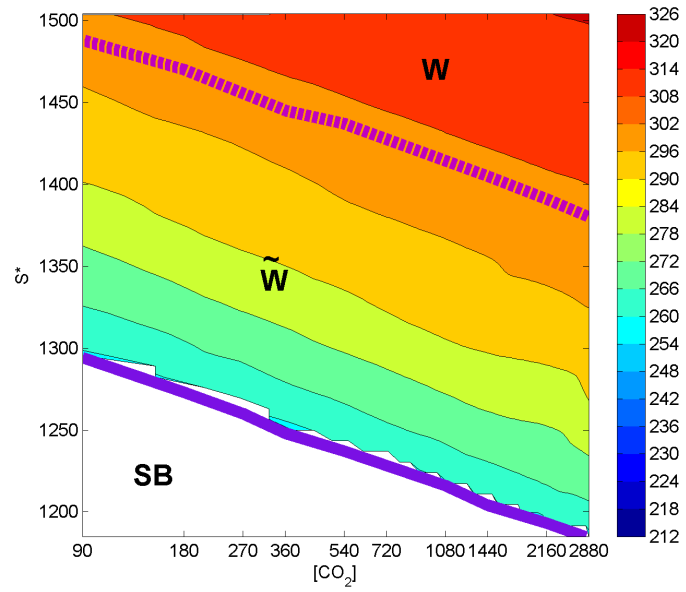


(a)

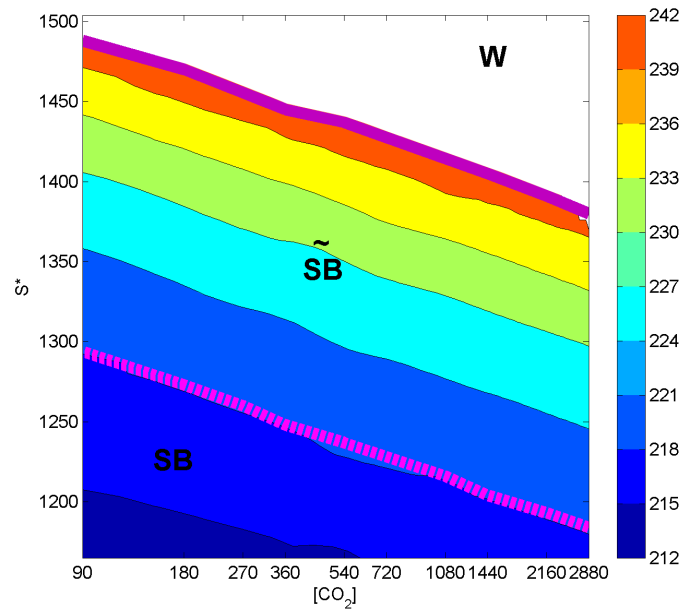


(b)

Figure 1:

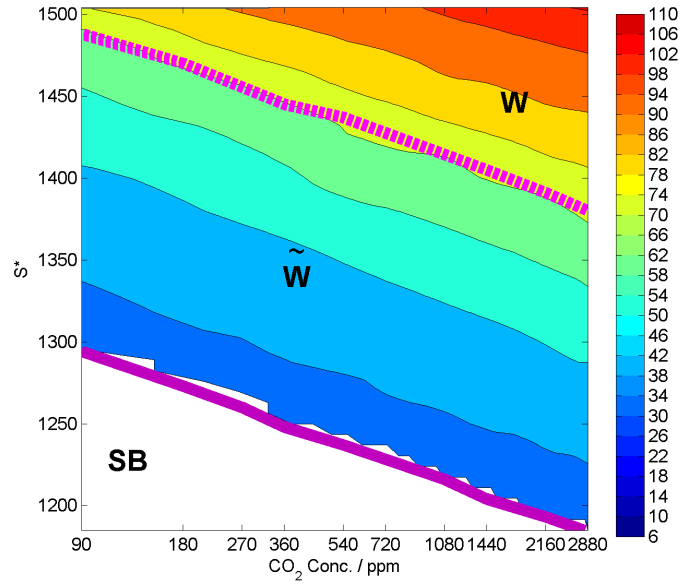


(a)

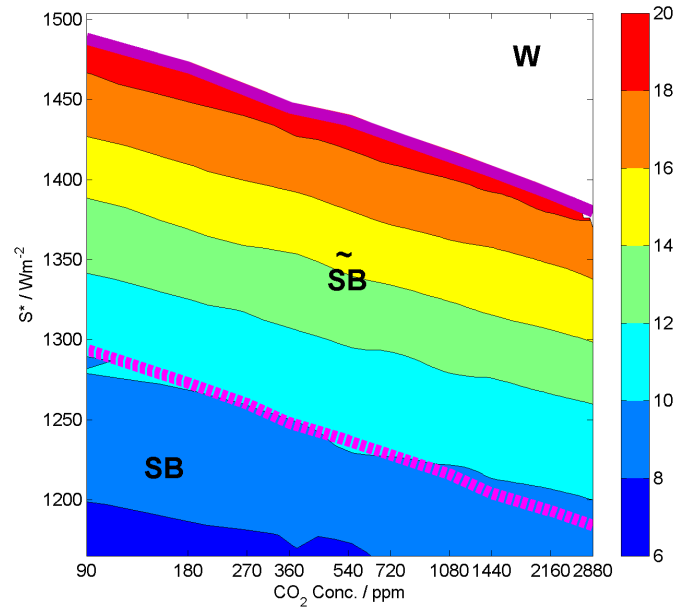


(b)

Figure 2:

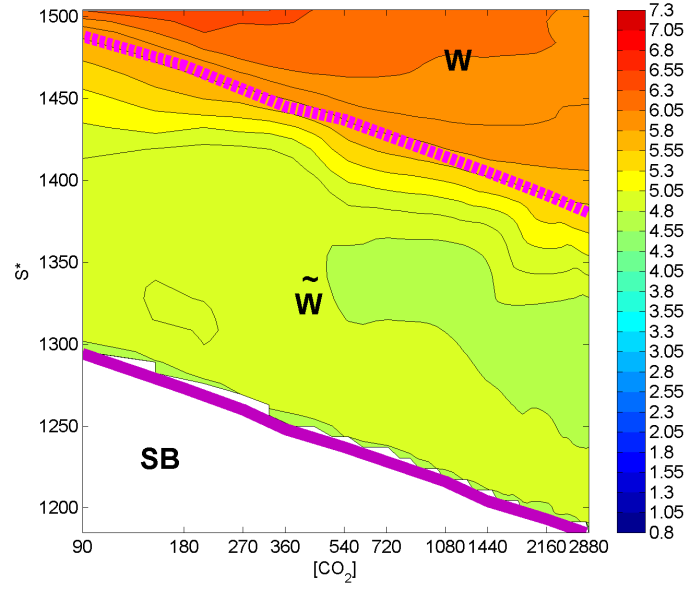


(a)

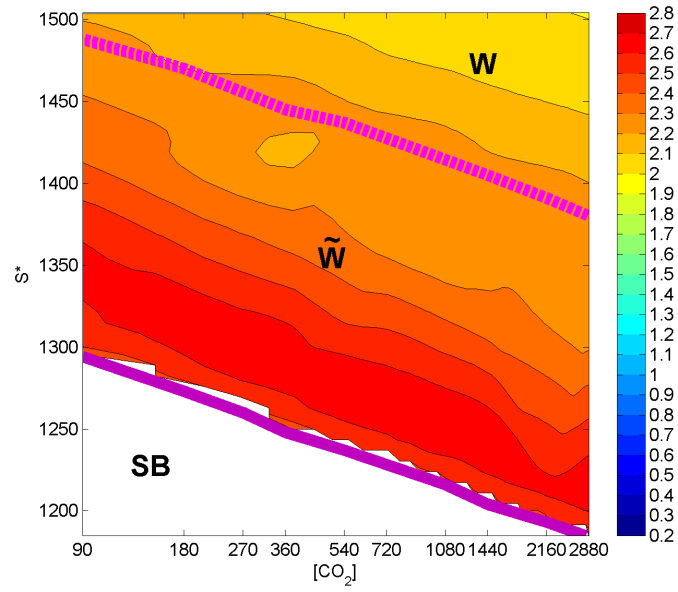


(b)

Figure 3:

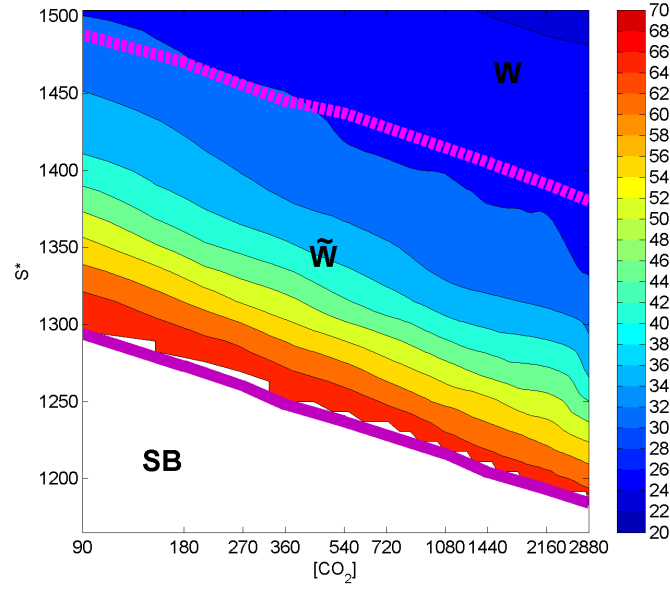


(a)

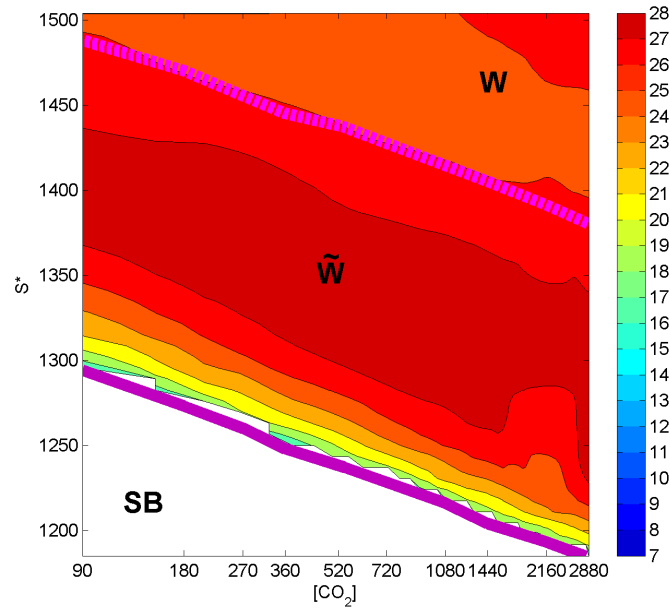


(b)

Figure 4:

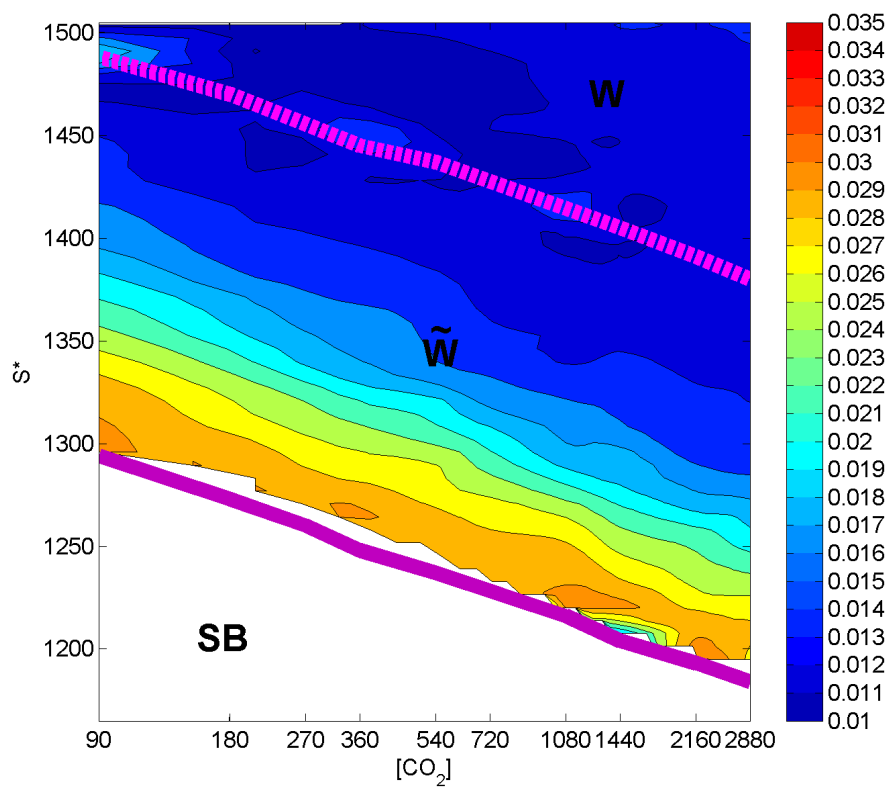


(a)



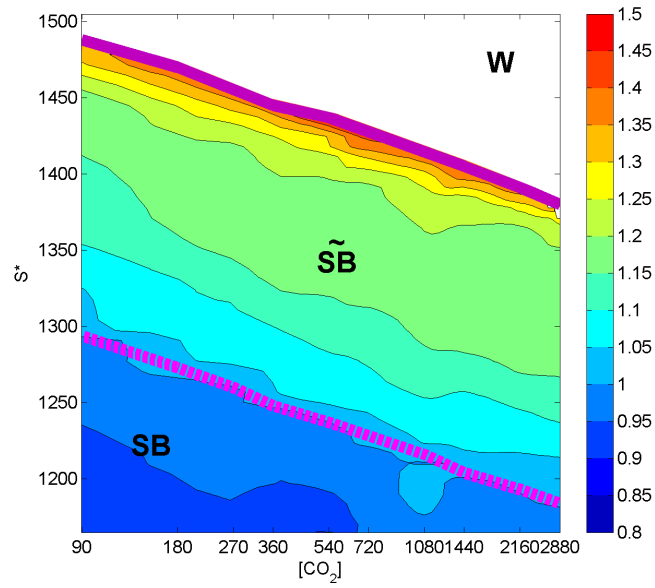
(b)

Figure 5:

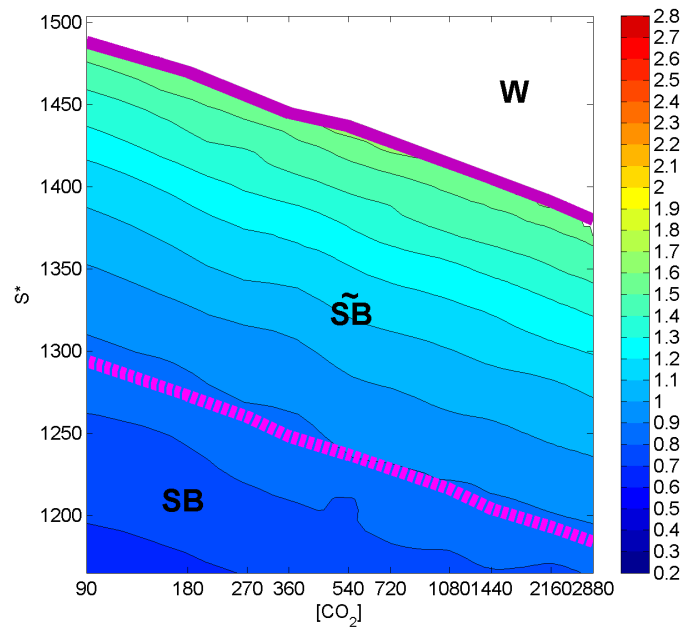


(a)

Figure 6:

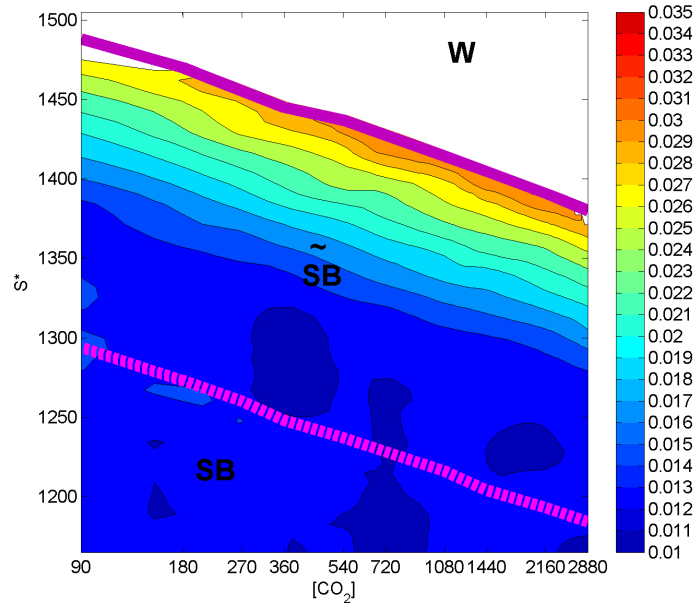


(a)

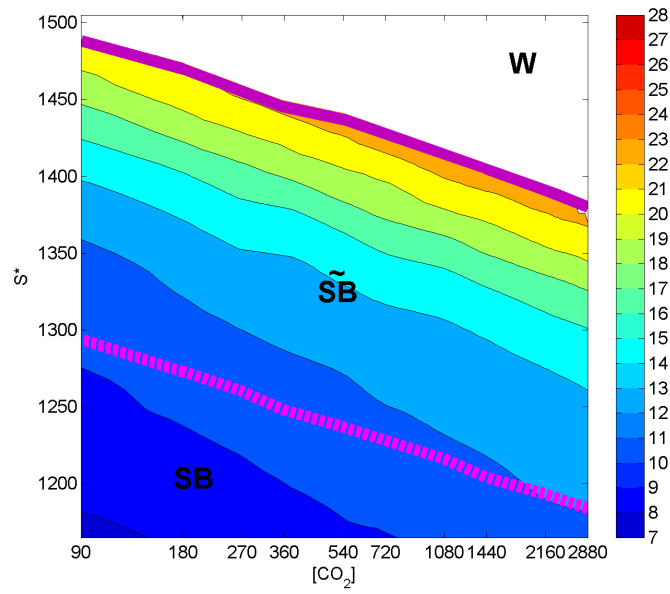


(b)

Figure 7:
40



(a)



(b)

Figure 8:

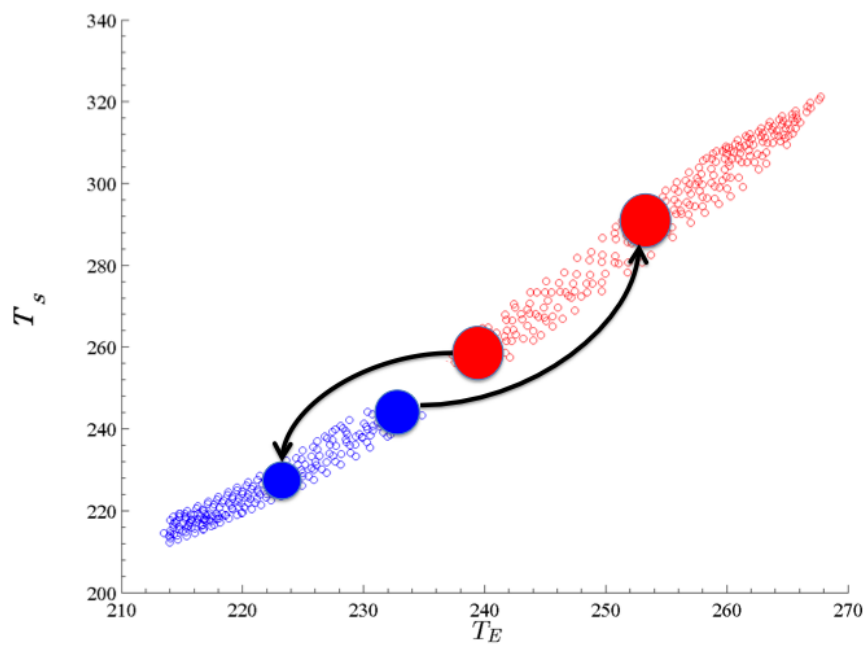
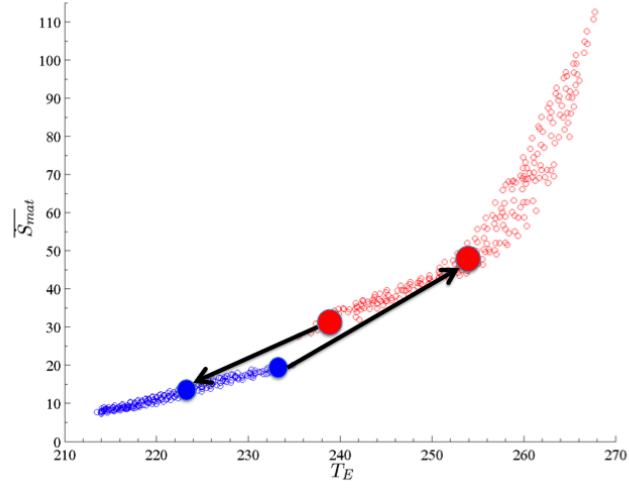
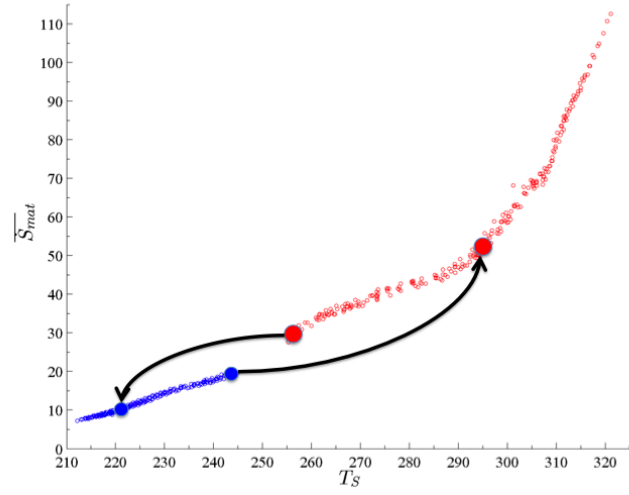


Figure 9:

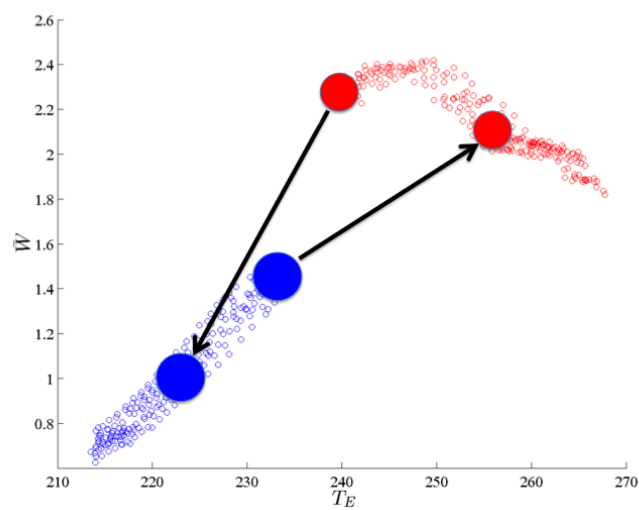


(a)

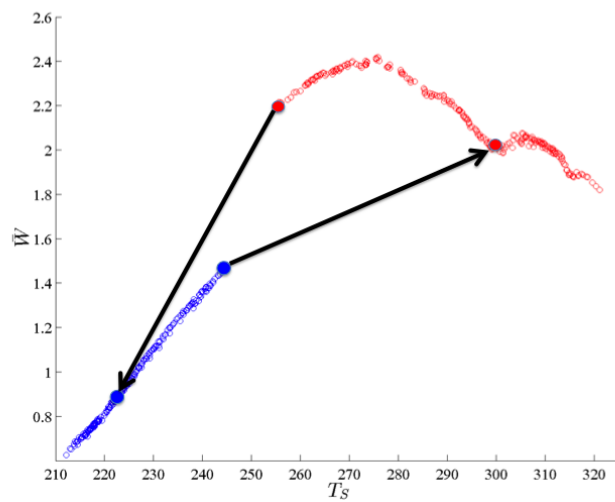


(b)

Figure 10:

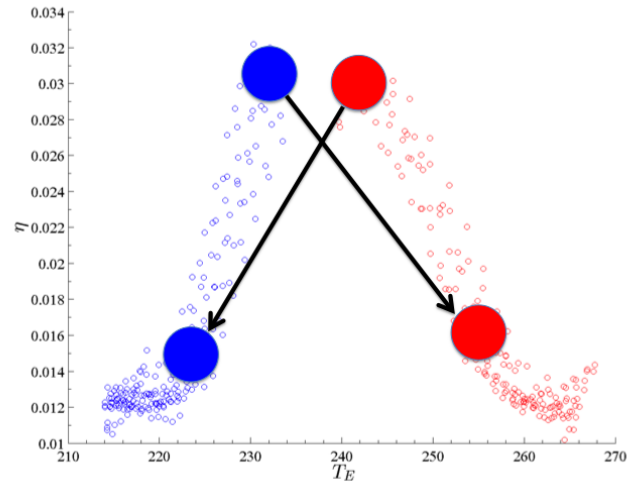


(a)

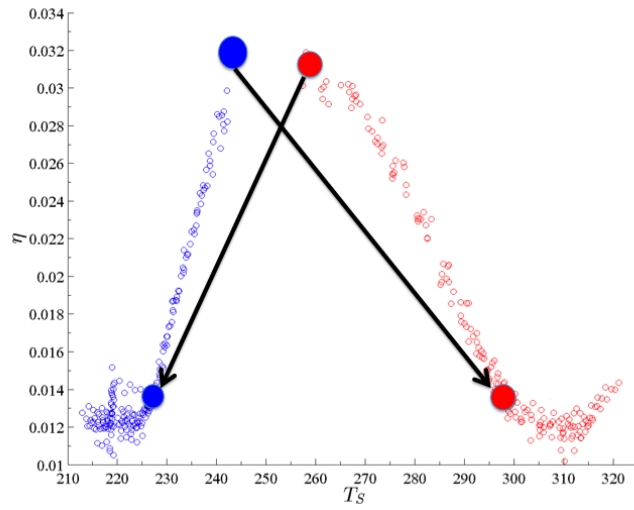


(b)

Figure 11:

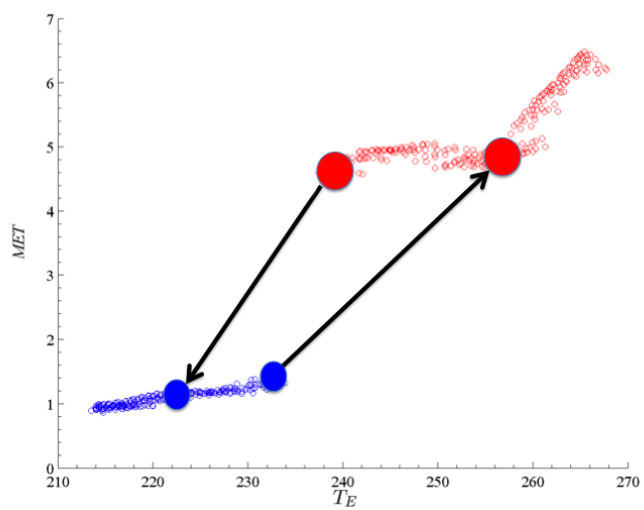


(a)

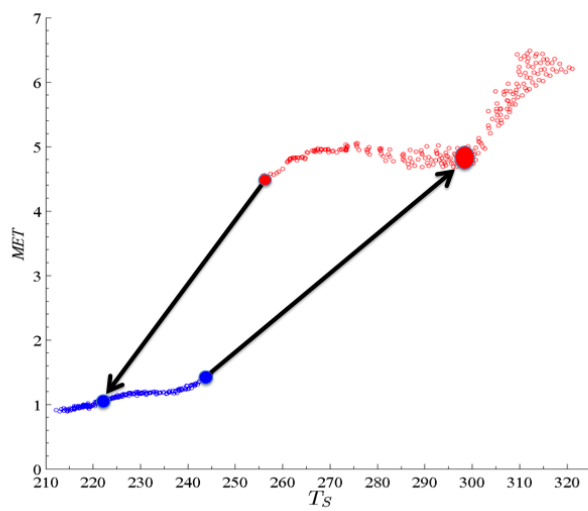


(b)

Figure 12:



(a)



(b)

Figure 13: